Article

Cell

A Cardiovascular Disease-Linked Gut Microbial Metabolite Acts via Adrenergic Receptors

Graphical Abstract

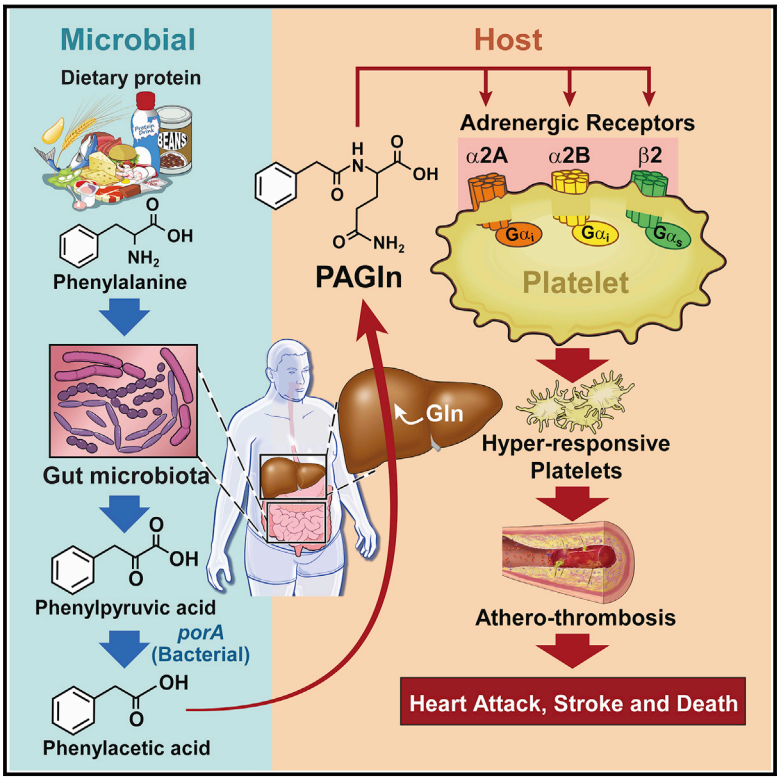

Highlights

- Gut microbe formed phenylacetyl glutamine (PAGln) contributes to cardiac disease
- Microbial *porA* and *fldH* impact host PAGln levels, platelet function, and thrombosis
- PAGln transmits cellular responses via the α2A, α2B, and β2 adrenergic receptors
- β blocker therapy attenuates PAGln-induced heightened thrombosis risk

Authors

Ina Nemet, Prasenjit Prasad Saha, Nilaksh Gupta, ..., Michael A. Fischbach, Joseph A. DiDonato, Stanley L. Hazen

Correspondence

hazens@ccf.org

In Brief

A microbially generated metabolite, PAGln, is associated with cardiovascular disease and death in humans. Studies in animal models provide insights into PAGln metabolism as well as its effects in driving platelet responsiveness and thrombosis through adrenergic receptors.

Nemet et al., 2020, Cell *180*, 862–877
March 5, 2020
https://doi.org/10.1016/j.cell.2020.02.016

CellPress

Cell

Article

A Cardiovascular Disease-Linked Gut Microbial Metabolite Acts via Adrenergic Receptors

Ina Nemet,[1,2,11] Prasenjit Prasad Saha,[1,2,11] Nilaksh Gupta,[1,2,11] Weifei Zhu,[1,2] Kymberleigh A. Romano,[1,2] Sarah M. Skye,[1,2] Tomas Cajka,[3,9] Maradumane L. Mohan,[1] Lin Li,[1,2] Yuping Wu,[4] Masanori Funabashi,[8,10] Amanda E. Ramer-Tait,[6] Sathyamangla Venkata Naga Prasad,[1] Oliver Fiehn,[3] Federico E. Rey,[7] W.H. Wilson Tang,[1,2,5] Michael A. Fischbach,[8] Joseph A. DiDonato,[1,2] and Stanley L. Hazen[1,2,5,12,*]

[1]Department of Cardiovascular & Metabolic Sciences, Lerner Research Institute, Cleveland Clinic, Cleveland, OH 44106, USA
[2]Center for Microbiome & Human Health, Cleveland Clinic, Cleveland, OH 44106, USA
[3]West Coast Metabolomics Center, University of California, Davis, Davis, CA 95616, USA
[4]Department of Mathematics, Cleveland State University, Cleveland, OH 44115, USA
[5]Heart and Vascular Institute, Cleveland Clinic, Cleveland, OH 44106, USA
[6]Department of Food Science and Technology, University of Nebraska-Lincoln, Lincoln, NE 68588, USA
[7]Department of Bacteriology, University of Wisconsin-Madison, Madison, WI 53706, USA
[8]Department of Bioengineering and ChEM-H, Stanford University, Stanford, CA 94305, USA
[9]Present address: Institute of Physiology of the Czech Academy of Sciences, Prague, 14200, Czech Republic
[10]Present address: Translational Research Department, Daiichi Sankyo RD Novare Co., Tokyo, 134–8630, Japan
[11]These authors contributed equally
[12]Lead Contact
*Correspondence: hazens@ccf.org
https://doi.org/10.1016/j.cell.2020.02.016

SUMMARY

Using untargeted metabolomics (n = 1,162 subjects), the plasma metabolite (*m/z* = 265.1188) phenylacetylglutamine (PAGln) was discovered and then shown in an independent cohort (n = 4,000 subjects) to be associated with cardiovascular disease (CVD) and incident major adverse cardiovascular events (myocardial infarction, stroke, or death). A gut microbiota-derived metabolite, PAGln, was shown to enhance platelet activation-related phenotypes and thrombosis potential in whole blood, isolated platelets, and animal models of arterial injury. Functional and genetic engineering studies with human commensals, coupled with microbial colonization of germ-free mice, showed the microbial *porA* gene facilitates dietary phenylalanine conversion into phenylacetic acid, with subsequent host generation of PAGln and phenylacetylglycine (PAGly) fostering platelet responsiveness and thrombosis potential. Both gain- and loss-of-function studies employing genetic and pharmacological tools reveal PAGln mediates cellular events through G-protein coupled receptors, including α2A, α2B, and β2-adrenergic receptors. PAGln thus represents a new CVD-promoting gut microbiota-dependent metabolite that signals via adrenergic receptors.

INTRODUCTION

Cardiovascular disease (CVD) remains the leading cause of death and morbidity in Western countries, and new therapeutic targets that contribute to CVD development and progression are needed. We hypothesized that studies in subjects with type 2 diabetes (T2DM) would prove fruitful in identifying novel pathways linked to CVD, since subjects with T2DM are both at markedly higher risk for development of CVD and its major adverse consequences (MACE, major adverse cardiac events = myocardial infarction (MI), stroke, or death) and suffer poorer prognoses and outcomes. Further, traditional CVD risk factors fail to adequately account for the heightened risks observed among subjects with T2DM. Interestingly, the degree of blood-glucose control within T2DM is a poor indicator of incident CVD risks, and numerous anti-diabetes medications lower plasma glucose levels without significantly impacting CVD development or MACE risks (Duckworth et al., 2009; Gerstein et al., 2001, 2008; Piarulli et al., 2009). These observations indicate that metabolic derangements distinct from glucose-related pathways occur with T2DM that contribute to the heightened CVD risks observed in this disorder.

Untargeted metabolomics is emerging as a powerful platform for discovery of pathways linked to diseases (Koh et al., 2018; Li et al., 2018; Lloyd-Price et al., 2019; Wang et al., 2011). This relatively unbiased approach enables development of a comprehensive list of circulating ionizable analytes associated with a given phenotype and whose chemical structures can be enumerated. However, structural identification of chemical signatures detected is challenging, and a significant portion of the spectral features observed within plasma remains of unknown structures (Blaženović et al., 2018; da Silva et al., 2015). Herein, we employed untargeted metabolomics analyses of plasma from subjects with T2DM, coupled with mechanistic investigations, to reveal a metabolite formed via a metaorganismal pathway enhanced in subjects with T2DM and associated with heightened CVD risks in both T2DM and non-diabetic subjects alike. The essential amino acid phenylalanine (Phe) serves as nutrient

precursor for the gut microbiota-generated metabolite phenylacetylglutamine (PAGln), which is both clinically and mechanistically linked to CVD and is shown to promote CVD-relevant phenotypes via host G protein-coupled receptors (GPCRs), including α2A, α2B, and β2-adrenergic receptors (ADRs).

RESULTS

Untargeted Metabolomics Identifies PAGln Is Associated with CVD

In an initial Discovery Cohort (n = 1,162; Table S1), untargeted metabolomics was performed on plasma from sequential stable subjects undergoing elective diagnostic cardiac evaluation with longitudinal (3 years) follow-up, as described under STAR Methods. Plasma analytes were prioritized based on three screening inclusion criteria: (1) association with incident (3 years) major adverse cardiac events (MACE = myocardial infarction (MI), stroke, or death), (2) heightened levels in T2DM, and (3) poor correlation with indices of glycemic control (Table S2). Of the spectral features in plasma monitored, the top MACE-associated predicted analytes were prioritized into two lists: those of known structures versus those of unknown structures at the time of analysis. The top 5 identified ("known") compounds included trimethylamine-*N*-oxide (TMAO) and trimethyllysine (TML), compounds linked to gut microbiota metabolism and incident CVD risks (Koeth et al., 2013; Li et al., 2018; Tang et al., 2013; Wang et al., 2011), along with three diacylglycerophospholipids with tentative structural identification (Table S2). Among "unknown" compounds, the top MACE-associated candidate (high resolution *m/z* 265.1188) fulfilled all three screening inclusion criteria and showed a hazard ratio (HR) 95% (confidence interval [CI]) for incident (3 years) MACE risk of 2.69 (1.61–4.52); $p < 0.0001$ (Figures 1A and 1B; Table S2). The *m/z* 265.1188 plasma analyte was then unambiguously identified as PAGln by multiple approaches, including demonstrating identical high resolution MS/MS spectra and retention time with authentic synthetic standard material on multiple stationary phases and chromatography conditions, both with and without derivatization, both in plasma and following isolation (Figure 1C; Figure S1; Table S3).

Untargeted metabolomics analyses are only semiquantitative and require both verification and more quantitative analyses of candidates to corroborate observed associations. We therefore developed a stable isotope dilution liquid chromatography with tandem mass spectrometry (LC/MS/MS) assay to quantify PAGln in an independent (non-overlapping) Validation Cohort (n = 4,000) of stable subjects undergoing elective diagnostic cardiac evaluation (Table S4). Within the entire cohort, higher plasma PAGln levels were observed among subjects with T2DM ($p = 0.0002$ versus non-diabetics), as well as among subjects with MACE ($p < 0.0001$ versus nonMACE). Kaplan-Meier survival analyses revealed subjects with high PAGln levels have greater incident (3 years) MACE risks (Figure 1D; $p < 0.0001$ log rank for all groups examined). Specifically, subjects with PAGln levels in the fourth quartile (Q4) versus those in the first (Q1) demonstrated a significantly increased risk of incident (3 years) MACE among both diabetics and non-diabetics alike (all subjects [HR, 2.80; 95% CI, 2.17–3.61], T2DM [HR, 2.73; 95% CI, 1.84–4.05], and non-diabetics [HR, 2.18; 95% CI, 1.59–3.00]; Figure 1E). Moreover, higher PAGln levels remained an independent predictor of incident MACE risks following adjustments for traditional cardiac risk factors (Figure 1E).

Gut Microbiota Participate in Production of PAGln and Phenylacetylglycine *In Vivo*

A gut microbial contribution to PAGln generation in humans was established by demonstrating marked suppression ($p < 0.0001$) of systemic PAGln levels in subjects (n = 15) in studies analyzing plasma at baseline (Pre-Abx), then following a 7-day course of oral poorly absorbed broad spectrum antibiotics cocktail (Abx) previously shown to suppress gut microbiota (Tang et al., 2013), and finally following a washout period (≥3 weeks) to permit repopulation of conventional human gut commensals (Post-Abx; Figure 2A). Previous studies with either liver extracts or isolated enzymes have reported PAGln can be formed by phenylacetic acid (PAA) conjugation to the amino acid glutamine (Gln) by both human and rhesus monkey liver enzymes (Webster et al., 1976), while other studies have shown PAA can be produced by bacterial fermentation of the essential amino acid Phe in culture (Dodd et al., 2017). In addition to PAGln, PAA conjugation to the amino acid glycine (Gly)-generating phenylacetylglycine (PAGly) has also been noted (González-Guardia et al., 2015; Wang et al., 2013). We therefore evaluated the physiological distribution of Gly versus Gln derivatives of PAA in apparently healthy subjects (n = 25), as well as in mice, where mechanistic studies would be performed. In humans, circulating levels of PAGln were found to be over an order of magnitude higher than PAGly. In contrast, PAGly levels in mice were an order of magnitude higher than PAGln (Figure 2B), and PAA administered via intraperitoneal (i.p.) injection was shown to be predominantly metabolized into PAGly (Figure 2C). Comparisons of serum levels of PAGly in conventionally reared versus germ-free (GF) mice, or before versus after oral cocktail of Abx exposure, showed that gut microbiota are a critical participant in PAGly formation from PAA (Figures 2B and 2D). Thus, in both humans and mice, PAGln and PAGly are produced *in vivo* via a metaorganismal pathway wherein dietary Phe is converted into PAA by gut microbiota, at which point host conjugation reactions occur with either Gln (preferred in humans) or Gly (preferred in rodents), producing PAGln and PAGly, respectively (Figure 2E).

PAGln Enhances Platelet Stimulus-Induced Calcium Release and Responsiveness to Multiple Agonists

The observed positive association between PAGln levels and incident thrombotic events in humans (Figure 1) suggested a potential effect of PAGln on platelet function and interactions with vascular matrix. We thus investigated whether PAGln impacted platelet adhesion to collagen surfaces in whole blood under physiological shear forces, using methods as previously described (Zhu et al., 2016). Studies were performed using PAGln levels observed in subjects within our clinical Validation Cohort, which is comprised of subjects with relatively preserved renal function (Tables S4 and S5). Exposure (30 min) of whole blood recovered from healthy volunteers (all confirmed to have low [< 4th quartile PAGln levels])

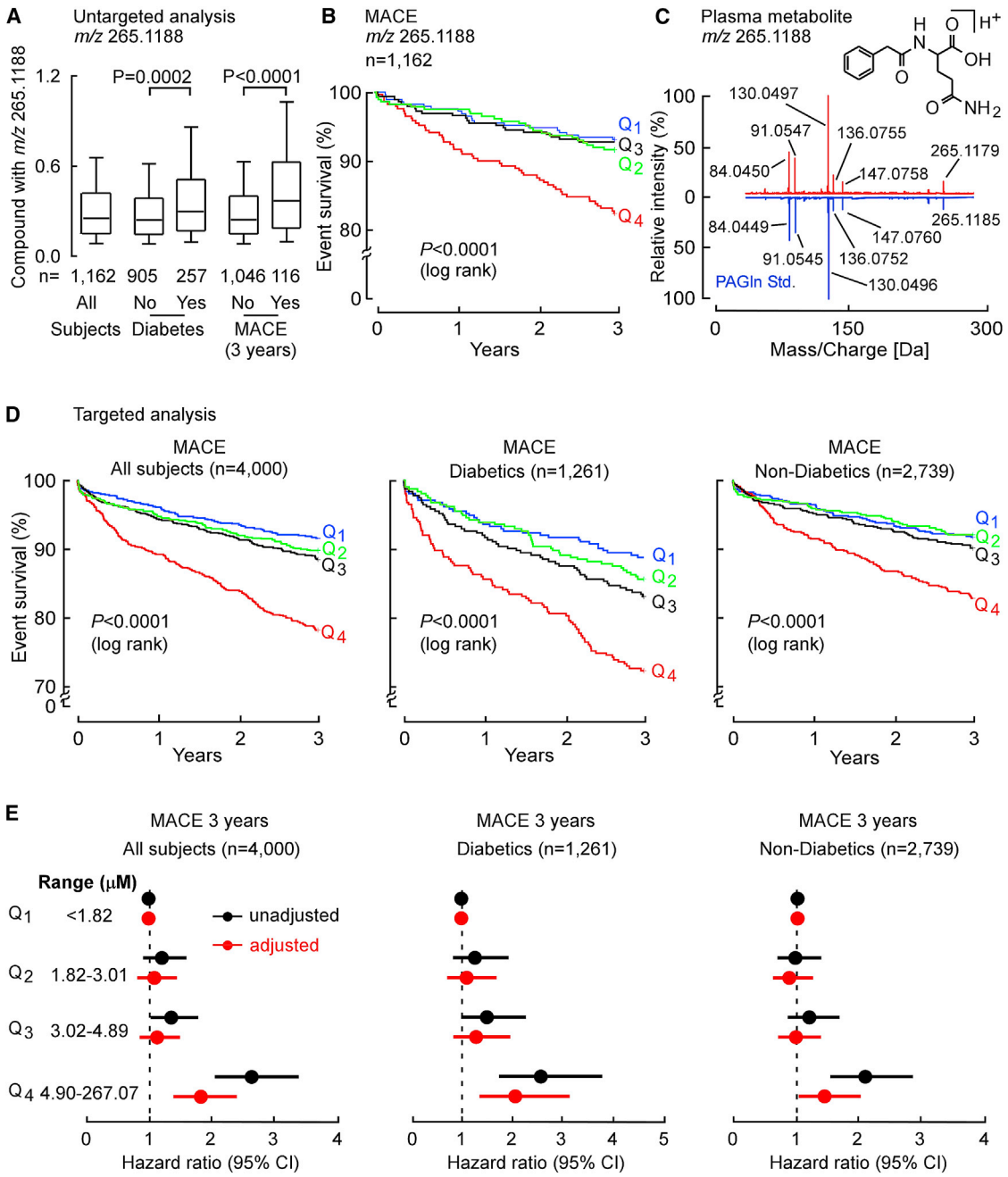

Figure 1. Untargeted Metabolomics Studies Discover that a Metabolite with *m/z* of 265.1188 Is Associated with Cardiovascular Disease Risk, Subsequently Identified as Phenylacetylglutamine

(A) Relative plasma levels of compound with *m/z* 265.1188 in sequential stable subjects undergoing elective diagnostic cardiac evaluation. Subjects (n = 1,162) were divided into groups based on whether they were diabetic or experienced an incident major adverse cardiac event (MACE: myocardial infarction [MI], stroke, or death) over the 3-year follow-up. In the box-whisker plot, the upper and lower boundaries of the box represent the 25th and 75th percentiles, the median is marked by a horizontal line inside the box, and whiskers represent 10% and 90% of measured values. Significance was determined by Mann-Whitney test.

(B) Kaplan-Meier estimates and the risk of MACE ranked by quartile of candidate analyte *m/z* 265.1188.

(C) Comparison of high-resolution collision-induced dissociation (CID) mass spectra of the metabolite *m/z* 265.1188 in plasma (red) and synthetic PAGln standard (blue).

(D) In the Validation Cohort (n = 4,000) and indicated sub-cohorts, Kaplan-Meier estimates and the risk of MACE according to PAGln quartile levels as measure by stable isotope dilution LC-MS/MS.

(legend continued on next page)

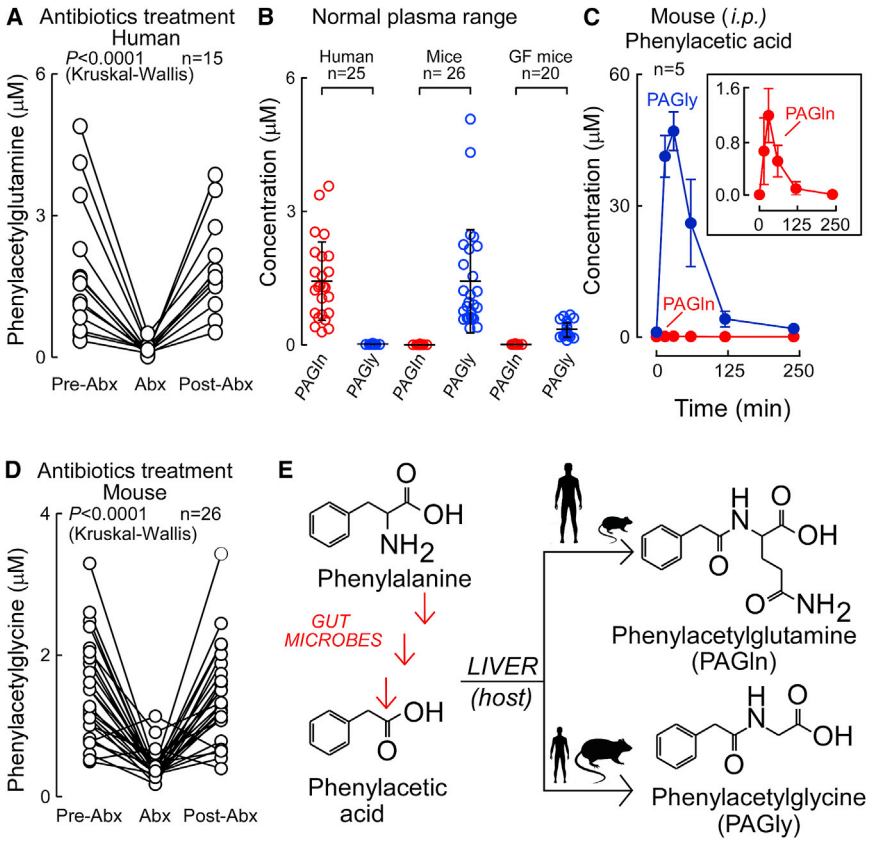

Figure 2. PAGln Production *In Vivo* Is a Microbiota-Dependent Process in Humans and Mice

(A) Fasting plasma levels of PAGln in subjects (n = 15) (1) before oral treatment with a cocktail of poorly absorbable, broad spectrum antibiotics (Pre-Abx), (2) after seven days of antibiotics regimen (Abx), and (3) three weeks after discontinuation of antibiotics (Post-Abx). Kruskal-Wallis test was used for the statistical analysis.

(B) Fasting plasma levels of PAGln and PAGly (mean ± SD) in indicated numbers of healthy human subjects (n = 25, left), conventionally raised mice (n = 26, mid) and GF mice (n = 20, right).

(C) Serial plasma levels of PAGln and PAGly after i.p. injection of phenylacetic acid (50 mg/kg; n = 5) in mice.

(D) Levels of PAGln in (n = 11) male and (n = 15) female mouse plasmas (1) before use of oral broad spectrum antibiotic cocktail (Pre-Abx), (2) after five days of antibiotics treatment (Abx), and (3) one week post antibiotics discontinuation (Post-Abx). Kruskal-Wallis test was used for the statistical analysis.

(E) Schematic outlining metaorganismal production of PAGln and PAGly in humans and mice.

to physiologically relevant levels of PAGln (both 10 μM and 100 μM; see Table S5 for distribution of PAGln levels in subjects within the Validation Cohort) substantially accelerated the rate of collagen-dependent platelet adhesion and spreading observed under physiological shear flow (Figures 3A–3C). Further, within whole blood, PAGln (10 μM [$p < 0.0001$] and 100 μM [$p < 0.0001$]) also induced enhancement in the adhesion of P-selectin-positive platelets on collagen matrix under physiological shear flow (Figure S2A). Brief (30 min) pretreatment of human platelet-rich plasma (PRP) with PAGln (100 μM) versus saline (vehicle) revealed PAGln significantly enhanced stimulus-dependent platelet aggregation to submaximal concentrations of three different known platelet agonists: ADP, thrombin receptor-activated peptide (TRAP6), and collagen ($p < 0.0001$ for ADP [Figure 3D, left]; $p = 0.003$ for TRAP6 [Figure S2C, left], and $p = 0.02$ for collagen [Figure S2C, right]). When a fixed submaximal level of each of the platelet agonists (ADP, TRAP6, or collagen) was used, PAGln was observed to dose-dependently enhance the extent of platelet aggregation in PRP across the physiological range of concentrations of PAGln found in our clinical cohort ($p = 0.016$ for ADP [Figure 3D, right; Figure S2B]; $p = 0.002$ for TRAP6 [Figure S2D, left], and $p = 0.018$ for collagen [Figure S2D, right]). In studies with washed human platelets, PAGln also dose-dependently enhanced submaximal ADP-stimulated P-selectin surface expression (Figure 3E) and glycoprotein $\alpha_2\beta_3$ (GP IIb/IIIa) activation (Figure 3F), with significant increases in platelet activation phenotypes noted with PAGln levels of 10 μM or greater.

The above results collectively suggested PAGln might directly interact with platelets, enhancing stimulus-dependent rise in intracellular cytosolic Ca^{2+} concentrations ($[Ca^{2+}]_i$). To directly test this, isolated human platelets were recovered from healthy donors and loaded with the calcium-selective dye Fura 2-AM, and the effect of PAGln on $[Ca^{2+}]_i$ was monitored in real time before versus following thrombin-induced activation. Pre-incubation of platelets with PAGln alone had no effect on baseline $[Ca^{2+}]_i$ levels (Figure 3G, left). However, exposure to physiological levels of PAGln dose-dependently enhanced submaximal (0.02 U) thrombin-evoked augmentation of $[Ca^{2+}]_i$ (Figure 3G). Similar results were observed with PAGly (Figures S2E–S2G). The above data demonstrate that the gut microbiota-dependent metabolites PAGln and PAGly significantly impact platelet function, enhancing platelet adhesion to collagen matrices and both platelet stimulus-dependent rise in $[Ca^{2+}]_i$ and aggregation in response to agonists.

(E) Risk of MACE by 3 years among all test subjects (n = 4,000, left), diabetics (n = 1,261, mid), and non-diabetics (n = 2,739, right) according to PAGln quartile levels using a multivariable Cox proportional hazard model. Unadjusted hazard ratio (black) and adjusted model (age, gender, smoking, HDL, LDL, triglyceride level, systolic blood pressure, and C-reactive protein level; red). The 5%–95% confidence intervals (CI) are indicated by the line length. See also Figure S1 and Tables S1–S5.

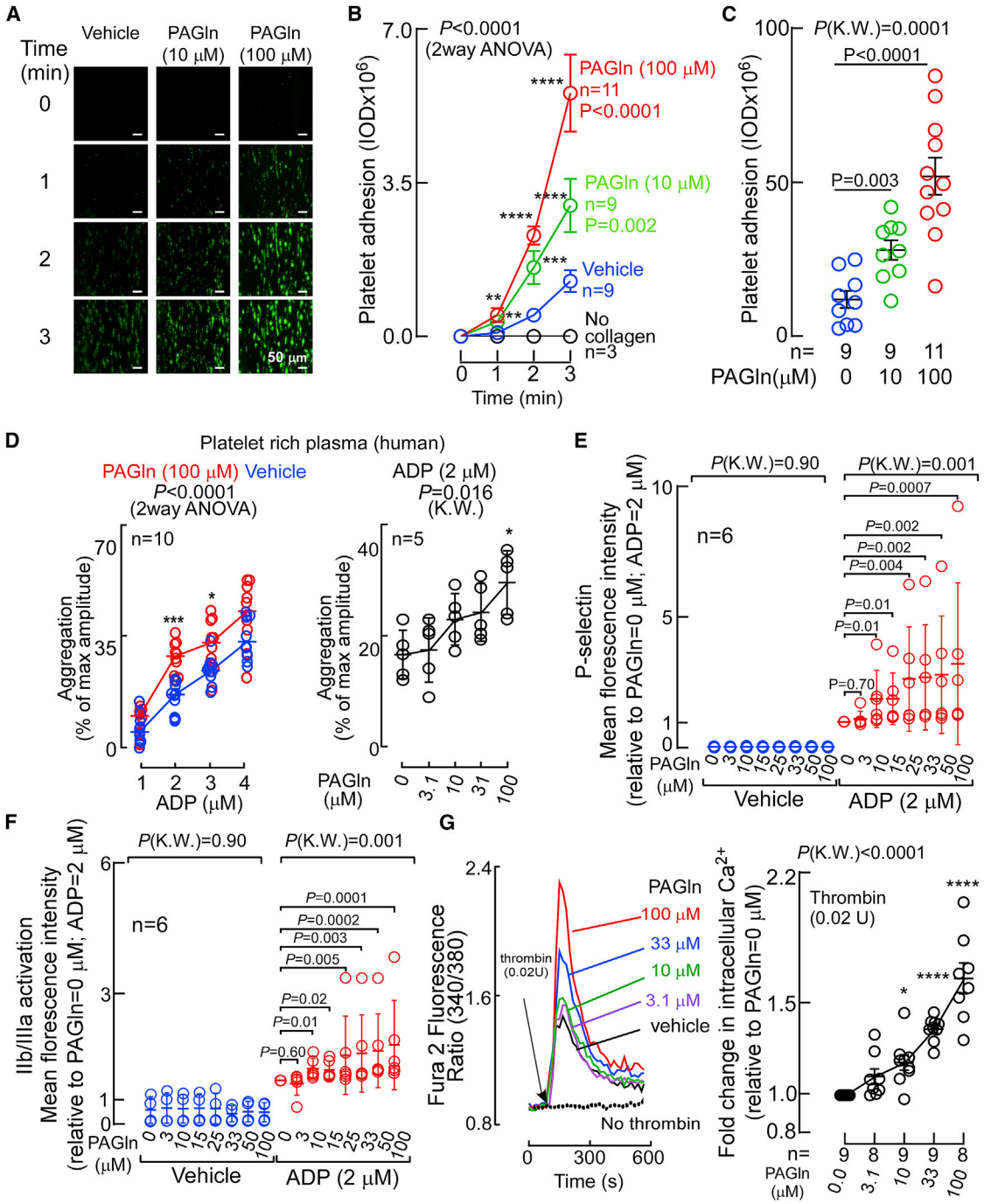

Figure 3. PAGln Enhances Platelet Responsiveness

(A) Human platelet adhesion in whole blood to a microfluidic chip surface (± collagen coating) under physiological shear conditions ± PAGln. Representative images of platelet (green) adhesion at the indicated times (scale bar, 50 μm).

(B) Adherent platelet integrated optical density (IOD, area x intensity) from whole blood recorded from the indicated number of subjects.

(C) Adherent platelet IOD at end point (i.e., after 3 min), in 5 high-power fields (per treatment and per subject) along the length of the channel (n = 9–11 as indicated).

(D) ADP-stimulated platelet aggregometry responses (n = 10) with fixed concentration of PAGln (100 μM, red) versus normal saline (vehicle, blue) (left) or varying concentrations of PAGln (n = 5) (fixed submaximal level of ADP [2 μM], right).

(E) ADP (versus vehicle)-induced changes in P-selectin surface expression in washed human platelets pre-incubated with the indicated concentrations of PAGln (n = 6).

(F) ADP (versus vehicle)-induced activation of platelet GP IIb/IIIa as assessed by PAC-1 antibody staining on washed human platelets pre-incubated with PAGln (n = 6).

(legend continued on next page)

PAGln Accelerates Platelet Clot Formation and Enhances Thrombosis Potential *In Vivo*

The impact of PAGln and PAGly on clot formation *in vivo* was examined using the $FeCl_3$-induced carotid artery injury model, a commonly used experimental approach to induce thrombosis. PAGln or PAGly were individually acutely raised by i.p. injections in mice (Figure S3A), and both the rate of platelet clotting following carotid artery injury and the time to cessation of flow within the carotid artery were quantified. Notably, both PAGln and PAGly each induced heightened platelet thrombus formation within the injured carotid artery (Figure 4A), and correspondingly reduced the time to cessation of blood flow following injury (i.e., the occlusion time) when compared to mice treated with the nutrient precursor Phe or normal saline (vehicle) (Figure 4B).

Gut Microbial Genes *porA* and *fldH* Modulate Host Thrombosis Potential *In Vivo*

We next tested whether the commensals and genes that contribute to PAGln/PAGly generation within hosts can modulate platelet function and thrombosis potential *in vivo*. Based on a combination of prior studies (Dickert et al., 2002; Dodd et al., 2017; Elsden et al., 1976), we illustrate in Figure S3B a schematic of proposed metaorganismal metabolic pathways for initial anaerobic conversion of dietary Phe into either PAA (oxidative pathway) or phenylpropionic acid (PPA, reductive pathway), followed by host-catalyzed Gln or Gly condensation with PAA forming PAGln or PAGly, respectively. Recent studies reported a role for the microbial *porA* gene in oxidative metabolism of Phe to PAA by the human commensal *Clostridium sporogenes* (Dodd et al., 2017). In addition, Elsden and colleagues previously reported PPA was a major product of Phe metabolism by clostridia (Elsden et al., 1976), and Dodd and colleagues also characterized a 15kb gene cluster in *C. sporogenes* that harbors a phenyllactate dehydratase (*fldABC*) (Dickert et al., 2002), along with adjacent genes (e.g., *fldH*), that were shown to be critical to catalytic reductive metabolism of aromatic amino acids including Phe (Dodd et al., 2017). The scheme (Figure S3B) is also based on PAA metabolism in humans and other mammals previously studied due to its use as an acute emergency treatment for hyperammonemia in patients with urea-cycle disorders, facilitating nitrogen removal as PAGln via urinary excretion (Brusilow et al., 1980; Webster et al., 1976). We therefore generated *C. sporogenes* mutants lacking either a functional *porA* or *fldH* gene, as described under STAR Methods. Because of the ability of *C. sporogenes* to generate trimethylamine, an alternative gut microbiota-derived metabolite that is precursor of the pro-thrombotic metabolite TMAO (Skye et al., 2018; Zhu et al., 2016), both *porA* or *fldH* mutants were generated in a Δ*cutC* background. To functionally characterize the mutants, they were cultured under anaerobic conditions in the presence of [$^{13}C_9$,$^{15}N_1$]-Phe, and generation of [$^{13}C_8$]-PAA versus [$^{13}C_9$]-PPA was determined by LC/MS/MS. As shown in Figure 4C, while (Δ*cutC*)*C. sporogenes* harboring both functional *porA* and *fldH* genes only generated isotope-labeled PPA and not PAA, the Δ*cutC*,Δ*fldH* mutant (still possesses functional *porA*) no longer generated PPA but did generate PAA (Figure 4C). In contrast, the (Δ*cutC*,Δ*porA*)*C. sporogenes* mutant (still possessing functional *fldH*) no longer generated PAA and only formed PPA. We then directly tested the impact of gut microbial PAA generation on host *in vivo* thrombosis potential by colonizing GF mice with either (Δ*cutC*)*C. sporogenes* or the (Δ*cutC*,Δ*fldH*)*C. sporogenes* mutants. Following microbial colonization, plasma levels of PAGly were determined from samples recovered at time of *in vivo* thrombosis assessment using the $FeCl_3$-induced carotid artery injury model (STAR Methods). Colonization of *C. sporogenes* strains post inoculation was confirmed by PCR of DNA extracted from cecal contents at the time of sacrifice. As predicted by the *in vitro* culture data (Figure 4C), colonization of the GF mice with (Δ*cutC*,Δ*fldH*)*C. sporogenes* resulted in significantly higher levels of PAGly ($p < 0.001$) than that observed in (Δ*cutC*)*C. sporogenes* colonized mice (Figure 4D). Following arterial injury, both the rate of thrombus generation and the time to cessation of blood flow within the injured vessel were significantly reduced in the mice colonized with the (Δ*cutC*,Δ*fldH*)*C. sporogenes* mutant, producing higher levels of PAA and consequently, PAGly (Figure 4D).

PAGln Shows Saturable and Specific Binding to Cells, Suggesting Specific Receptor-Ligand Binding Interaction

Since PAGln directly fosters cellular effects at physiological levels, we next sought to decipher underlying molecular participants that might contribute to PAGln-elicited cellular events. To test whether PAGln shows evidence of binding to a cellular receptor(s), we used dynamic mass redistribution (DMR), a label-free technology based on refractive index changes that enables real-time detection of ligand-dependent integrated cellular responses in live cells (Schröder et al., 2010, 2011). Addition of PAGln to the human bone marrow-derived megakaryoblasts (MEG01), a culturable precursor cell of platelets, resulted in a positive DMR response similar to known receptor binding ligands like norepinephrine (Norepi) and collagen, which bind to ADRs and the glycoprotein VI (GPVI) receptor (Leitinger, 2011; Small et al., 2003), respectively, and acted as positive controls. In contrast, the PAGln precursor (and structural analog) Phe, which does not bind to a legitimate cell receptor, displayed no DMR response (similar to vehicle control), and was used as negative control (Figure S4A). Examination of increasing concentrations of potential binding ligands (PAGln versus Norepi versus Phe) with MEG01 cells demonstrated saturable and specific DMR dose-response curves, typical for a ligand-receptor interaction process with PAGln and Norepi but not Phe (Figure 5A). In parallel studies, saturable and specific DMR dose-response signal was also observed following PAGln binding to the human bone marrow-derived erythroleukemia cells (HEL92.1.7; Figure S4B).

(G) (Left) Representative fluorescent signal showing thrombin-induced changes in intracellular calcium concentration [Ca^{2+}] in Fura 2-filled washed human platelets incubated with PAGln. (Right) Fold-change (relative to PAGln = 0 μM) in peak Fura 2 fluorescence following submaximal (0.02 U) thrombin stimulation at the indicated concentrations of PAGln in washed human platelets (n = 8–9 as indicated). Data points represent the mean ± SEM (n = biological replicates). Significance was measured with nonparametric one- or two-way ANOVA with multiple comparisons (*$p < 0.05$; **$p < 0.01$; ***$p < 0.001$; ****$p < 0.0001$). See also Figure S2.

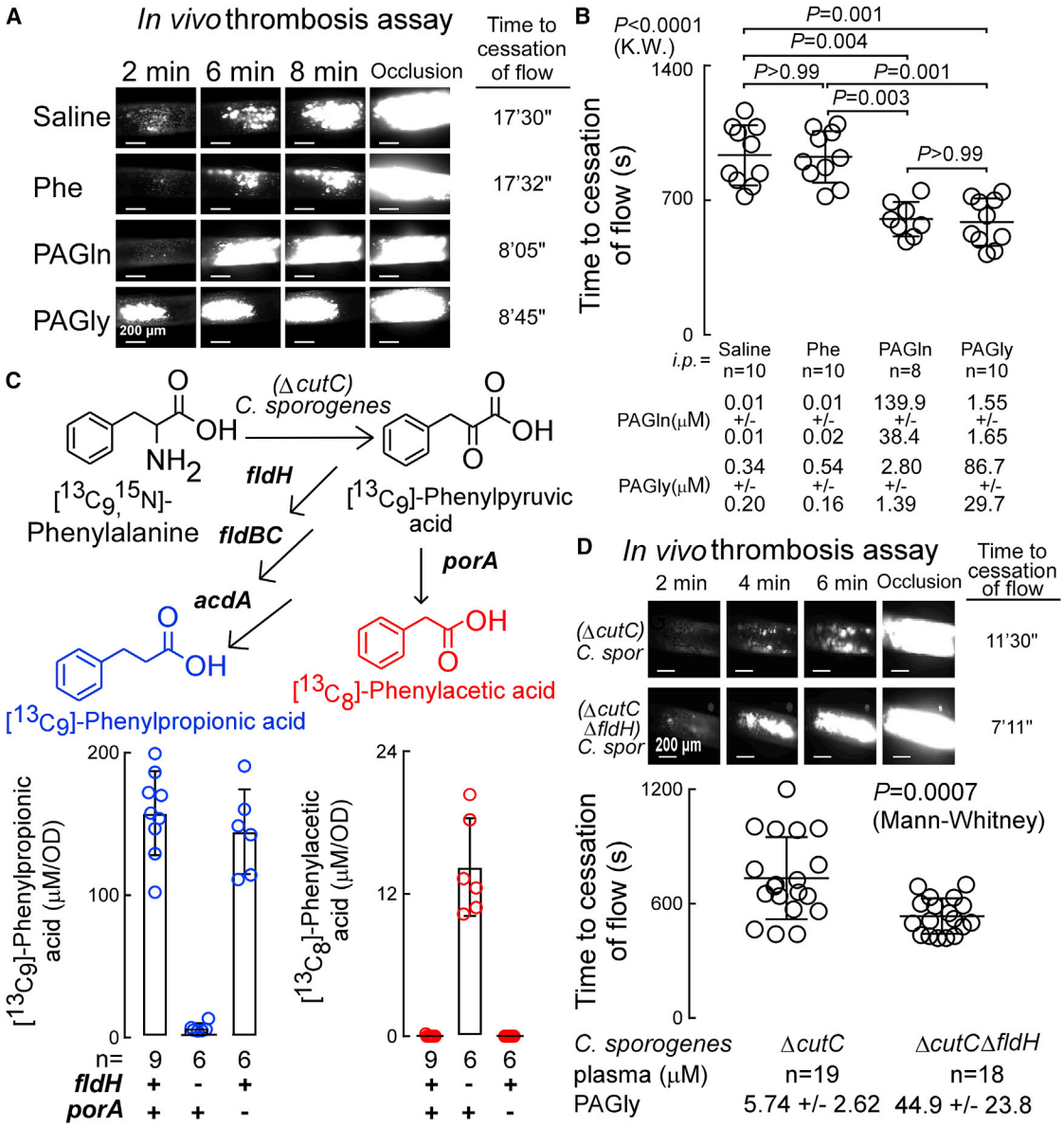

Figure 4. PAGln and PAGly Enhance *In Vivo* Thrombosis Potential

(A) Representative pictographs of carotid artery thrombus formation at the indicated time points following $FeCl_3$-induced carotid artery injury (scale bar, 200 µm).

(B) Time to cessation of blood flow in mice from indicated groups (mean ± SEM; nonparametric Mann-Whitney test for non-pairwise and Kruskal-Wallis test for multiple comparisons).

(C) Synthesis of phenylacetic acid (PAA) and PPA by *C. sporogenes* Δ*cutC* mutant with a disrupted gene for reductive metabolism of Phe (Δ*fldH*) were compared to (Δ*cutC*)*C. sporogenes* mutant with a disrupted gene for oxidative metabolism of Phe (Δ*porA*). *C. sporogenes* mutants were incubated with synthetic [$^{13}C_9$,^{15}N]-Phe and production of [$^{13}C_8$]-PAA (red) and [$^{13}C_9$]-PPA (blue) was measured in the indicated number of replicates (n = 6–9 as indicated) and results of each normalized by optical density (OD).

(D) Time to cessation of blood flow in GF mice mono-colonized with (Δ*cutC*)*C. sporogenes* (n = 19) or (Δ*cutC*,Δ*fldH*)*C. sporogenes* (n = 18) mutants. Shown are (top) representative pictographs of carotid artery thrombus formation at the indicated time points following arterial injury (scale bar, 200 µm), and (bottom) time to cessation of blood flow in mice from the indicated groups. Bar and whiskers represent mean ± SEM time to cessation of blood flow within the indicated group. See also Figure S3.

PAGln Mediates Cellular Events via G Protein-Coupled Receptors

Since PAGln demonstrates receptor-ligand interaction properties with cells, we next tested whether PAGln-induced DMR cellular responses were impacted by known GPCR signaling pathway modulators like pertussis toxin (PTX), cholera toxin (CTX), and YM-254890, which mask activation of $G\alpha_{i/o}$, $G\alpha_s$, and $G\alpha_q$ subunit-mediated signaling pathways, respectively

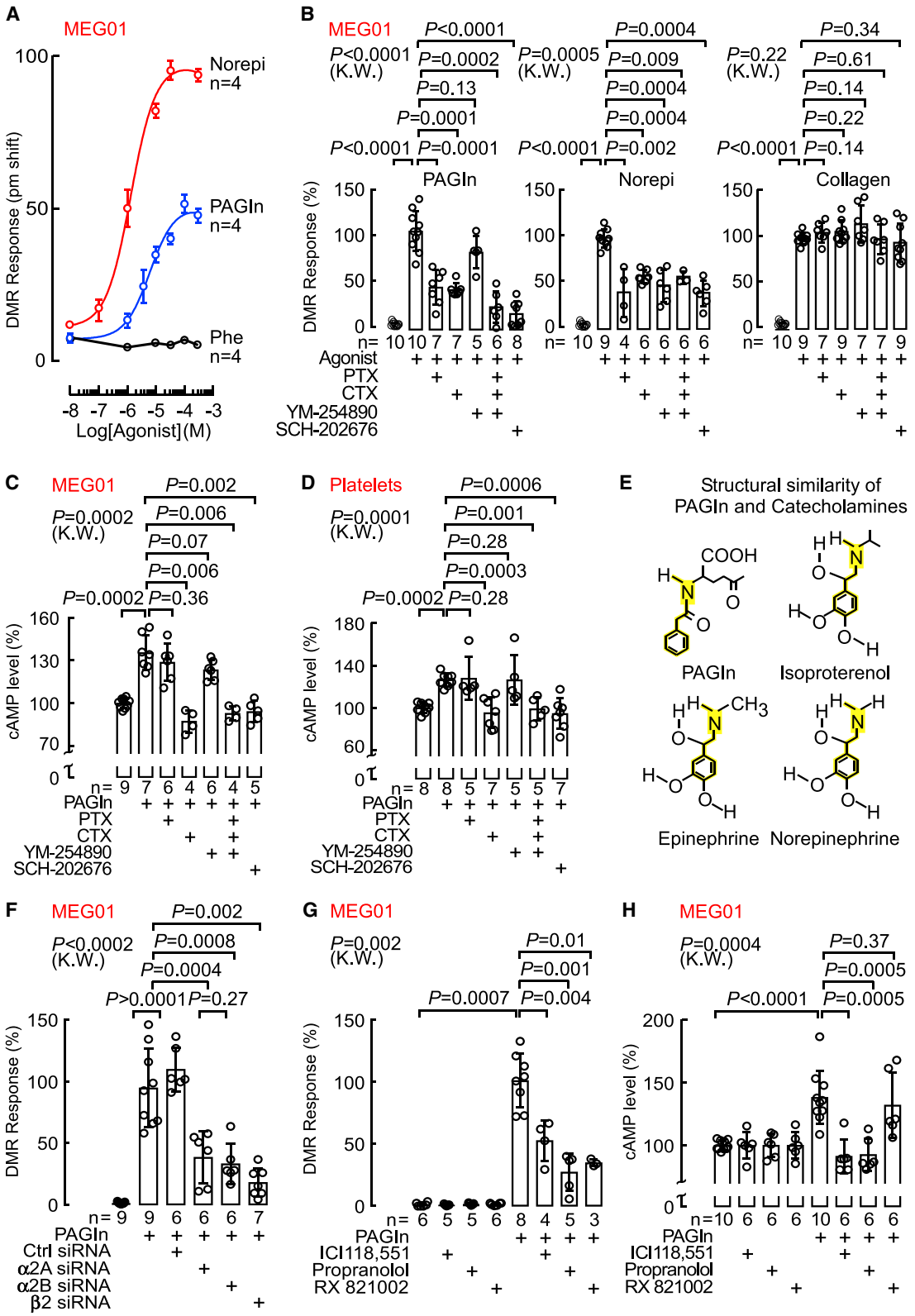

(legend on next page)

(Campbell and Smrcka, 2018; Milligan and Kostenis, 2006). Additionally, we examined PAGln-induced DMR cellular responses in the absence or presence of SCH-202676, a global GPCR inhibitor that blocks both agonist and antagonist binding to structurally diverse GPCRs that couple to $G\alpha_{i/o}$, $G\alpha_s$, and $G\alpha_q$ proteins (Fawzi et al., 2001; Lewandowicz et al., 2006). As positive control, we used Norepi as a GPCR binding ligand, while collagen (a non-GPCR binding ligand) was used as negative control. The PAGln-induced DMR response in MEG01 cells was significantly reduced by pretreating the cells with either a combination of all three modulators (PTX, CTX, and YM-254890) or by use of the global GPCR inhibitor SCH-202676, strongly implicating GPCR involvement in PAGln responses by the cells (Figure 5B, left; Figures S4C and S4D, left). Further, pretreatment of cells with either PTX or CTX, but not YM-254890, significantly suppressed the PAGln-induced DMR response, suggesting $G\alpha_{i/o}$ and $G\alpha_s$ involvement (Figure 5B, left; Figure S4C). Moreover, examination of DMR responses to Norepi, which is known to signal through all three of the aforementioned G-protein subunits to variable degrees (Hein, 2006), showed significant reduction in DMR signal upon incubations with each of the known GPCR modulator agents (Figure 5B, middle). In contrast, the DMR signal with collagen (negative control), remained unaffected by pretreatment of cells to each of the known GPCR modulator agents (Figure 5B, right). GPCR involvement in PAGln-induced DMR responses were also indicated in HEL.92.1.7 cells, where a similar effect of these G-protein modulators was observed, though unlike in MEG01, the $G\alpha_q$ modulator YM-254890 also displayed a significant reduction in PAGln-induced DMR response (Figure S4E).

The above data suggest PAGln-induced DMR responses in MEG01 and HEL92.1.7 cells appear to be mediated via saturable and specific responses to one or more GPCRs. We therefore examined whether PAGln elicited detectable changes in either intracellular cAMP or $[Ca^2]_i^+$. As we previously noted with platelets (Figure 3G), in the absence of other agonists, PAGln alone had no direct effect on $[Ca^{2+}]_i$ in either MEG01 (Figure S5A) or HEL92.1.7 cells (Figure S5B). But PAGln did elicit a modest (approx. 20%–30%) yet significant ($p = 0.0002$ for each) transient (within 5 min) increase in cAMP in both MEG01 cells (Figure 5C; Figure S5C) and washed human platelets (Figure 5D; Figure S5D). Moreover, pretreatment of each with known GPCR modulators showed CTX or the global GPCR inhibitor SCH-202676 inhibited PAGln-evoked cAMP production, suggesting PAGln exposure triggered $G\alpha_s$-mediated activation of adenylyl cyclase (Figures 5C and 5D; Figure S5E, S5F, and S4D, right). Isoproterenol (ISO), which predominantly binds to β2-ADRs that primarily couple to the $G\alpha_s$ subunit in both MEG01 cells (Figure S5G) and in platelets (Figure S5H) (Koryakina et al., 2012), was used as a positive control. Collectively, these data indicate PAGln mediates cellular responses through GPCR(s) in multiple cells, including isolated human platelets.

The Gut Microbiota-Dependent Metabolite PAGln Acts via ADRs

Given that PAGln mediates cellular responses via GPCR(s), we next sought to determine their identity. While more than 800 distinct GPCRs exist within the human genome, we noted that PAGln has a somewhat similar structure to catecholamines known to bind to the large multi-gene family of ADRs (Figure 5E). Because ADRs possess a flexible agonist pocket (Masureel et al., 2018), we hypothesized that PAGln may induce cellular signaling through ADRs, focusing on family members present on human platelets (α2A, α2B, and β2 ADRs) (Anfossi and Trovati, 1996; Barnett et al., 1985; Colman, 1990). We initially performed loss-of-function studies in MEG01 cells using both genetic and pharmacological approaches. PAGln-induced DMR responses were monitored following transfection with either control scrambled siRNAs or siRNA targeting either α2A, α2B, or β2 ADRs. Importantly, we confirmed >50% reduction in MEG01 cell mRNA levels of either *ADR2A*, *ADR2B,* or *ADRB2* following siRNA targeting of either α2A, α2B, or β2 ADRs, respectively, but no reduction following scrambled siRNAs (Figure S6A). Notably, each of the siRNAs against the three ADRs demonstrated a significant reduction in PAGln-induced DMR response in MEG01 cells while control siRNA had no effect (Figure 5F). Positive control (DMR response of epinephrine [Epi], which binds to all the aforementioned platelet ADRs to various extent [Hein, 2006]) showed significant reduction in DMR signal with siRNA knockdown of α2A, α2B, or β2 ADRs, but not with the control scrambled siRNA (Figure S6B). Further, the same ADR targeting siRNAs showed no effect on MEG01 DMR responses following exposure to a non-ADR binding ligand, ATP (Figure S6C).

In complementary studies, we used pharmacological inhibitors against the known ADRs in human platelets (α2A, α2B, or β2 ADRs): the selective β2 antagonist ICI118,551, the nonselective

Figure 5. PAGln Mediates Cellular Response through G-Protein Coupled Receptor(s) and via ADRs

(A) DMR dose response of PAGln, Norepi, and Phe in MEG01 cells (n = 4; max DMR responses after ligand addition).

(B) DMR response of PAGln (100 μM, left), Norepi (10 μM, middle), and collagen (10 μg/mL, right) in MEG01 cells pre-treated with the G-protein modulators PTX (100 ng/mL), CTX (1 μg/mL), YM-254890 (0.5 μM), or SCH-202676 (1 μM) (n = 5–10 as indicated).

(C and D) cAMP levels in (C) MEG01 cells and (D) washed human platelets pretreated with PAGln (100 μM, 5 min), in presence of PTX (100 ng/mL), CTX (1 μg/mL), YM-254890 (1 μM), or SCH-202676 (1 μM). cAMP levels were normalized to 100% immediately before addition of PAGln (n = 4–9 as indicated).

(E) Structure similarity between PAGln and catecholamines (ISO, Epi, and Norepi).

(F) DMR response in MEG01 cells transfected with control scrambled siRNAs and siRNAs against the α2A, α2B, and β2 ADRs and analyzed under indicated conditions (n = 6–9 as indicated). Maximum DMR response to PAGln was normalized to 100%.

(G) PAGln (100 μM) DMR response quantified in MEG01 cells treated with 10 μM selective β2 antagonist ICI118,551, nonselective β-blocker propranolol or nonselective α2 antagonist RX821002 for 30 min (n = 3–8 as indicated). The maximum DMR response to PAGln was normalized to 100%.

(H) cAMP levels in MEG01 cells after PAGln (100 μM, 5 min) treatment in the presence of 10 μM ICI118,551, propranolol, or RX821002 (n = 6–10 as indicated). cAMP levels were normalized to 100% in all treatments immediately prior to addition of PAGln. Nonparametric Mann-Whitney test was used for non-pairwise comparisons and Kruskal-Wallis test for multiple comparisons. Data points represent the mean ± SEM (n = biological replicates). See also Figure S4–S6.

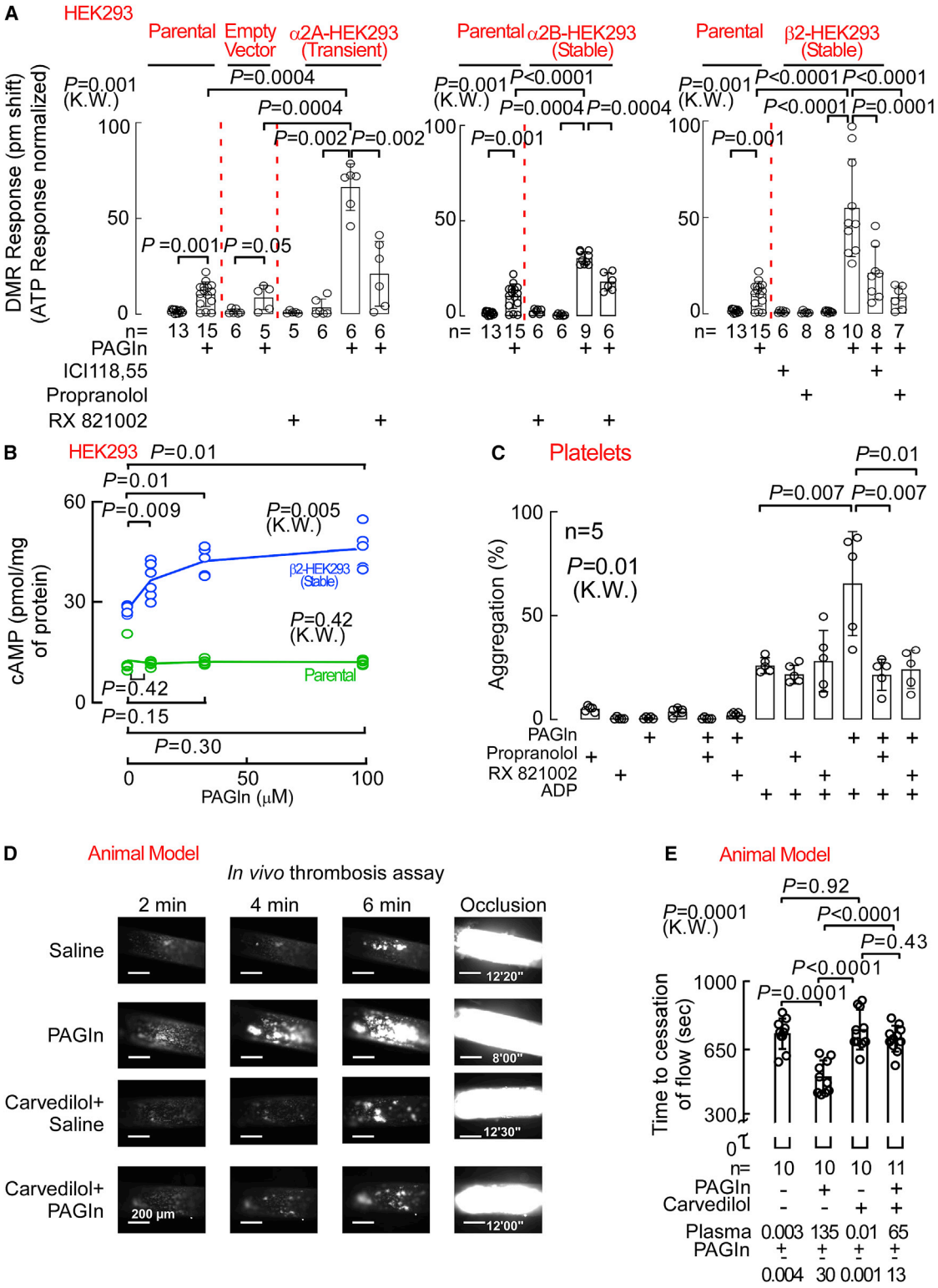

Figure 6. PAGln Modulates Platelet Function and *In Vivo* Thrombosis Potential via ADRs

(A) PAGln (100 μM) DMR response in parental HEK293, EV-transfected HEK293, *ADRA2A*-transfected HEK293 (left), α2B-HEK293 stably expressing (middle), and in β2-HEK293 stably expressing cells (right) after treating the cells with 10 μM ICI118,551, propranolol, or RX821002 for 30 min (n = 5–15 as indicated).

(B) cAMP levels in parental HEK293 and in β2-HEK293 stably expressing cells after PAGln treatment for 10 min (n = 4–6 as indicated).

(legend continued on next page)

β-blocker propranolol, and the nonselective α2 antagonist RX821002 (Atwood et al., 2011; Bilski et al., 1983; O'Rourke et al., 1994). The DMR response induced by PAGln incubation with MEG01 cells was substantially reduced by each of the aforementioned inhibitors, while the inhibitors alone did not affect the DMR response (Figure 5G). As positive control, the DMR response of the β2 agonist ISO was diminished in presence of either ICI118,551 or propranolol, and the DMR response of the α2 agonist B-HT933 was inhibited with RX821002 (Figure S6D). The DMR response to the non-ADR binding ligand ATP remained unchanged in the presence of ADR inhibitors (Figure S6E). Finally, ICI118,551 and propranolol, but not RX821002, inhibited PAGln (5 min exposure)-induced cAMP production in both MEG01 cells (Figure 5H) and platelets (Figure S6F). Similarly, intracellular cAMP production after ISO treatment in MEG01 (Figure S6G, left) and washed human platelets (Figure S6G, right) was reduced with ICI118,551 or propranolol, but not with RX821002. Thus, both genetic and pharmacological loss-of-function studies confirm PAGln can induce cellular responses via α2A, α2B, and β2 ADRs.

Gain-of-Function Studies Confirm PAGln Can Signal via α2A, α2B, and β2 ADRs

To further confirm the capacity of PAGln to function through ADRs, we carried out gain-of-function studies by individually overexpressing α2A, α2B, and β2 ADRs in human embryonic kidney cells (HEK293), which were selected because of their relatively low endogenous level of ADR density (~34 fmol/mg protein as assessed by [^{125}I]-cyanopindalol binding; STAR Methods). While incubation of either parental or empty vector (EV)-transfected HEK293 cells with PAGln elicited nominal DMR responses, enhanced PAGln-evoked DMR responses were observed with HEK293 cells transfected either transiently with the ADRA2A gene (α2A-HEK293) or stably with either the ADRA2B gene (α2B-HEK293) or ADRB2 gene (β2-HEK293) (Figure 6A). Moreover, use of the above-mentioned selective ADR pharmacological inhibitors reversed the PAGln-induced DMR responses in the corresponding ADR expressing cells (i.e., the PAGln-induced DMR responses in α2A-HEK293 and α2B-HEK293 cells were reversed with RX821002, and the PAGln-induced DMR responses in β2-HEK293 cells were attenuated by either ICI118,551 or propranolol [Figure 6A]). As additional control studies, we performed similar experiments using the α2 agonist B-HT933 for α2A-HEK293 and α2B-HEK293 cells and observed an elevated B-HT933-elicited DMR response as compared to parental HEK293 cells, while responses were attenuated by RX821002 (Figure S7A). Likewise, the β2 agonist ISO displayed enhanced DMR response in β2-HEK293 cells, which were inhibited with either ICI118,551 or propranolol (Figure S7A). As an additional (negative) control, ATP-elicited DMR responses remained unaffected in all ADR transfected cells (α2A-HEK293, α2B-HEK293, and β2-HEK293) in the presence of the respective ADR inhibitors (Figure S7B). In complementary gain-of-function studies, we analyzed PAGln effects on cAMP levels. Notably, parental HEK293 cells showed no PAGln-evoked change in intracellular cAMP levels (green line), whereas β2-HEK293 cells showed significant PAGln-induced increases in cytosolic cAMP levels (blue line) (Figure 6B). In addition, PAGln dose-dependently increased cAMP production in *ADRB2* gene-transfected *Cricetulus griseus* hamster ovary (CHO-K1) cells, which also possess very low endogenous levels of β2 ADR (~29 fmol/mg receptor density; STAR Methods), similar to positive control ISO. Both PAGln- and ISO-induced cAMP production in the β2 ADR-transfected CHO-K1 cells was inhibited by addition of ICI118,551 (Figure S7C). Furthermore, $[Ca^{2+}]_i$ remained unaffected by PAGln exposure in all cells examined (Figures S8A–S8E). Thus, both loss-of-function and gain-of-function studies employing either genetic or pharmacological approaches in multiple cell types confirm that PAGln can induce cellular responses via α2A, α2B and β2 ADRs.

Platelet Hyperresponsiveness and Accelerated *In Vivo* Rate of Thrombus Generation Evoked by PAGln Are Attenuated with Select ADR Inhibitors

The above studies suggest that some of the potential benefits of ADR-blocking agents in CVD may arise from antagonism of PAGln-induced effects. Consistent with this, we observed exposure of PRP recovered from healthy volunteers with low PAGln levels to pathophysiologically relevant levels of PAGln augmented submaximal ADP-stimulated platelet aggregation responses. Concomitantly, PAGln exposure in the presence of either propranolol, ICI118,551, or RX821002 attenuated PAGln-induced platelet hyperresponsiveness (Figures 6C and S8F). Moreover, neither ADR inhibitor showed a direct effect on submaximal ADP-stimulated platelet aggregation response (but abolished the PAGln-heightened platelet aggregation response; Figure 6C). Thus, addition of each of the ADR inhibitors reversed PAGln-elicited platelet hyperresponsiveness.

In a final series of studies, we examined the effect of a widely used β-blocker in clinical practice, carvedilol (Gupta et al., 2004), on PAGln-induced enhancement in thrombus formation *in vivo*. Studies were performed as before (Figure 4), examining the impact of PAGln (acutely elevated via i.p. injection) on $FeCl_3$-induced arterial injury-provoked rate of the platelet thrombus formation and the time to vessel occlusion. However, this time we used mice in the absence versus presence of carvedilol (1.5 g/kg for one week). Notably, in the absence of β-blocker therapy, PAGln again both significantly accelerated the rate of platelet thrombus generation (Figure 6D) and shortened the time to cessation of blood flow (Figure 6E). While treatment of mice with carvedilol alone had no effect on *in vivo* thrombus

(C) ADP-stimulated platelet aggregometry responses in human PRPs (n = 5) pre-incubated with the 10 μM propranolol or RX821002 for 15 min prior to PAGln (100 μM) treatment for 30 min.

(D) Representative pictographs of carotid artery thrombus formation at the indicated time points following $FeCl_3$-induced carotid artery injury in mice i.p. injected with PAGln (or saline) and fed diet ± β-blocker carvedilol (1.5 g/kg; scale bar, 200 μm).

(E) Quantification of occlusive thrombosis for the indicated numbers of mice in each group. Plasma PAGln levels are noted at the bottom.

Nonparametric Mann-Whitney test was used for non-pairwise comparisons and Kruskal-Wallis test for multiple comparisons. Data points represent the mean ± SEM (n = 10–11 as indicated). See also Figures S7 and S8.

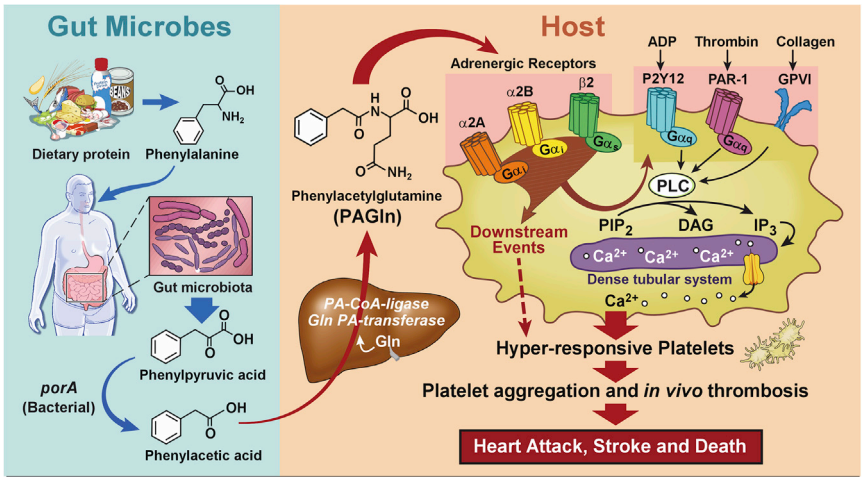

Figure 7. Gut-Microbial Metabolite PAGln Involvement in Enhancement of Platelet Thrombotic Potential via ADRs

A scheme summarizing the metaorganismal origins of PAGln, its recognition by ADRs, and its overall relationship with CVD as revealed through the studies presented is illustrated in Figure 7. Following ingestion of Phe, the majority of the essential amino acid is absorbed in the small intestines, but unabsorbed Phe that reaches the large intestines can be metabolized by gut microbiota to form phenylpyruvic acid (the initial microbiota-generated deamination product) and subsequently PAA. Following absorption into the portal system, PAA is readily metabolized in the liver to produce PAGln (major product in humans) and PAGly (major product in mice). PAGln has long been recognized as a synthetic product of PAA and Gln by liver and renal tissues of humans (Moldave and Meister, 1957), as well as a non-invasive probe of citric acid cycle intermediates in humans and primates (Yang et al., 1996). The present studies confirm a major role for gut microbiota in PAGln (and PAGly) generation in both humans and mice, as shown in studies with antibiotic cocktail to suppress gut microbiota and corroborative studies using GF versus conventionally reared mice. Notably, a limited number of recent studies have suggested an association between PAGln and some cardiometabolic phenotypes using semiquantitative analyses. For example, PAGln levels were noted to be substantially increased in subjects with end-stage renal disease (to more than 500 μM in some subjects [Meyer et al., 2016]) and associated with mortality in one study (Shafi et al., 2015). However, no association between PAGln and mortality was observed in another study of end-stage renal disease subjects, though significant elevation with renal disease was reported (Shafi et al., 2017). Elevated urinary levels of PAGln have also recently been associated with obesity (Elliott et al., 2015), early renal function decline (Barrios et al., 2015; Poesen et al., 2016), and diabetes (Loo et al., 2018; Urpi-Sarda et al., 2019). Despite these reports, a mechanistic link between PAGln and CVD pathogenesis has not yet been reported.

The present studies suggest several mechanisms through which the clinical association between heightened PAGln and incident CVD risks may occur. First, PAGln was shown to impact thrombosis potential through multiple complementary approaches. *Ex vivo* cellular studies using whole blood, PRPs, and isolated platelets all indicate that PAGln (and PAGly) enhance platelet function (enhanced stimulus-dependent responsiveness to multiple agonists and intracellular calcium release). Furthermore, numerous *in vivo* studies reveal that pathophysiologically relevant levels of PAGln or PAGly each facilitate both enhanced rate of thrombus formation and thrombosis potential in arterial injury models, including studies ranging from direct administration of either PAGln or PAGly to microbial transplantation studies

generation rate or time to cessation of blood flow following arterial injury ($p = 0.92$; Figure 6E), the pro-thrombotic effect of PAGln was reversed with carvedilol (Figures 6D and 6E).

DISCUSSION

Based on prior successes (Koeth et al., 2013; Koh et al., 2018; Li et al., 2018; Wang et al., 2011; Zhang et al., 2018), we hypothesized that using untargeted metabolomics as a discovery platform, coupled with functional studies, could serve as a relatively unbiased approach for revealing new metabolic pathways in humans that potentially contribute to the development of CVD and its adverse complications. To both enrich our potential pool of candidate metabolic derangements associated with incident CVD event risks and enhance the likelihood of uncovering a novel pathway, we elected to initially focus our studies on a vulnerable patient population at known heightened CVD risks but via unclear mechanisms—diabetics (i.e., the heightened CVD risks in T2DM are recognized to be, in part, via mechanisms distinct from traditional CVD risk factors and the degree of glucose control [Duckworth et al., 2009; Gerstein et al., 2001, 2008; Piarulli et al., 2009]). We thus sought to identify circulating metabolites that were increased in T2DM, associated with development of CVD, and poorly correlated with indices of glycemic control (i.e., fasting glucose, HgbA1C, glucose to insulin ratio). Remarkably, many of the top candidates identified that met these criteria proved to be mechanistically linked to gut microbiota (e.g., PAGln, TMAO, and TML; Tables S1 and S2; [Koeth et al., 2013; Tang et al., 2013; Wang et al., 2011; Zhu et al., 2016]). Moreover, PAGln (like TMAO and TML), was observed to be associated with incident CVD risks in both T2DM subjects and non-diabetic subjects alike. Thus, use of untargeted metabolomics, coupled with functional studies, has proven to be a valuable approach for discovery of new pathways clinically and mechanistically linked to CVD. Moreover, a remarkable proportion of metabolic candidates and pathways identified are linked to gut microbiome—the filter of our largest environmental exposure, that is, what we eat (Aron-Wisnewsky and Clément, 2016; Brown and Hazen, 2018; Jonsson and Bäckhed, 2017; Koeth et al., 2019; Koh et al., 2018; Koopen et al., 2016).

that modulate production of PAA, the precursor of PAGln (and PAGly). Notably, microbial engineering and transplantation studies into gnotobiotic mice reveal that the relative activity of the gut microbial *fldH* gene cluster versus the *porA* gene can regulate gut microbial production of PAA versus PPA, impacting PAGly production within the host. Critically, the balance between gut microbial activities of either the FldH versus PorA protein ultimately impacted the *in vivo* thrombosis potential in the colonized mice under gnotobiotic conditions, as monitored by both rate of thrombus formation and vessel occlusion time following arterial injury.

Another mechanism through which PAGln may impact CVD-relevant phenotypes is via its demonstrated interactions with GPCRs, including ADRs. Direct biophysical studies indicate saturable and specific binding of PAGln to cells, indicative of a cell receptor-ligand interaction, and studies with multiple complementary known GPCR inhibitors modulate PAGln mediated cellular responses and downstream signaling. A systematic series of genetic loss-of-function and gain-of-function studies, as well as multiple corroborative pharmacological inhibitor and agonist studies, unambiguously show PAGln can signal via α2A, α2B, and β2 ADRs—ADRs known to be expressed on platelets. Moreover, PAGln-elicited pro-thrombotic effects in a murine model of arterial injury were reversed by treatment of mice with a widely used β-blocker in clinical practice. In addition, studies with either specific ADR siRNA knockdown or ADR antagonists were both shown to block PAGln-induced pro-thrombotic phenotypes, further indicating PAGln can promote cellular signals via ADRs. β-Blocker therapy is known to foster numerous clinical benefits in some subjects with CVD (e.g., reduced risks of heart attack, stroke, heart failure, and death [Black et al., 2010; Burnett et al., 2017; Witte et al., 2018]). The present results suggest some of the clinical benefits observed with β-blocker therapy may in part be mediated via attenuation in PAGln-triggered ADR signaling events *in vivo*. It is notable that carvedilol has been shown to promote inhibition of platelet function in several trials (Petrikova et al., 2005; Ilardi et al., 2018), and the present studies suggest a potential mechanism through which this may occur. ADRs are widely expressed on virtually every cell type and known to play important roles in myocardial and vascular function, as well as regulation of body homeostasis in both health and pathologic states (Amrani and Bradding, 2017; Hein and Kobilka, 1997; Lefkowitz et al., 2000; Rockman et al., 2002). Activation of the adrenergic system also has a profound effect on metabolism, and prolonged activation can lead to insulin resistance, alterations in glucose and fatty acid metabolism, and mitochondrial dysfunction (Ciccarelli et al., 2013; Fu et al., 2017). Although the present studies currently focused only on three ADRs that are expressed in human platelets, one can speculate that PAGln has potential to modulate other ADRs, and accordingly, may potentially affect multiple ADRs—linked physiological processes *in vivo*.

STAR★METHODS

Detailed methods are provided in the online version of this paper and include the following:

SUPPLEMENTAL INFORMATION

Supplemental Information can be found online at https://doi.org/10.1016/j.cell.2020.02.016.

A video abstract is available at https://doi.org/10.1016/j.cell.2020.02.016#mmc2.

ACKNOWLEDGMENTS

This work is supported by grants from the NIH and Office of Dietary Supplements (P01HL147823, R01HL103866, R01HL126827) and the Foundation Leducq. K.A.R. was supported in part by NIH/NHLBI training grant HL134622. Mass spectrometry studies were performed on instrumentation housed in a facility supported in part through a Shimadzu Center of Excellence award and NIH shared instrumentation grant 1S10OD016346. Microfluidic shear flow experiments were done with the help from the Lerner Research Institute Imaging Core.

AUTHOR CONTRIBUTIONS

I.N., P.P.S., and N.G. designed, performed, and analyzed data from most of the studies and wrote the manuscript with input from all authors. T.C. and O.F. performed untargeted metabolic analysis; I.N. performed the mass spec analysis and compound identification; M.F. and M.A.F. performed genetic manipulation of *C. sporogenes*; K.A.R. helped with culturing bacteria and GF mouse experiments; and N.G., S.M.S., and W.Z. helped in the design and performance of platelet functional studies, *in vivo* thrombosis, and other mouse experiments. P.P.S. performed cell culturing and DMR signaling experiments. M.L.M. and S.V.N.P. helped with ADR experiments. A.E.R.-T. and F.E.R. provided GF mice. L.L. and Y.W. helped with statistical analysis. J.A.D. provided overall advice. W.H.W.T. and F.E.R. provided critical scientific input and discussions. S.L.H. conceived, designed, and supervised all studies and the drafting and editing of the manuscript. All authors contributed to the critical review of the manuscript.

DECLARATION OF INTERESTS

S.L.H. reports being named as co-inventor on pending and issued patents held by the Cleveland Clinic relating to cardiovascular diagnostics and therapeutics, being a paid consultant for P&G, having received research funds from P&G and Roche Diagnostics, and being eligible to receive royalty payments for inventions or discoveries related to cardiovascular diagnostics or therapeutics from Cleveland HeartLab, Quest Diagnostics, and P&G. The other authors have reported that they have no relationships relevant to the contents of this paper to disclose.

Received: August 8, 2019
Revised: December 16, 2019
Accepted: February 7, 2020
Published: March 5, 2020

REFERENCES

Gerstein, H.C.G., Miller, M.E., Byington, R.P., Goff, D.C., Jr., Bigger, J.T., Buse, J.B., Cushman, W.C., Genuth, S., Ismail-Beigi, F., et al. (2008). Effects of intensive glucose lowering in type 2 diabetes. N. Engl. J. Med. *358*, 2545–2559.

Amrani, Y., and Bradding, P. (2017). β2-Adrenoceptor Function in Asthma. Adv. Immunol. *136*, 1–28.

Anfossi, G., and Trovati, M. (1996). Role of catecholamines in platelet function: pathophysiological and clinical significance. Eur. J. Clin. Invest. *26*, 353–370.

Aron-Wisnewsky, J., and Clément, K. (2016). The gut microbiome, diet, and links to cardiometabolic and chronic disorders. Nat. Rev. Nephrol. *12*, 169–181.

Atwood, B.K., Lopez, J., Wager-Miller, J., Mackie, K., and Straiker, A. (2011). Expression of G protein-coupled receptors and related proteins in HEK293, AtT20, BV2, and N18 cell lines as revealed by microarray analysis. BMC Genomics *12*, 14.

Barnett, D.B., Swart, S.S., Nahorski, S.R., and Cook, N. (1985). Characterisation of human platelet adrenoceptors. Adv. Exp. Med. Biol. *192*, 97–108.

Barrios, C., Beaumont, M., Pallister, T., Villar, J., Goodrich, J.K., Clark, A., Pascual, J., Ley, R.E., Spector, T.D., Bell, J.T., and Menni, C. (2015). Gut-Microbiota-Metabolite Axis in Early Renal Function Decline. PLoS ONE *10*, e0134311.

Bilski, A.J., Halliday, S.E., Fitzgerald, J.D., and Wale, J.L. (1983). The pharmacology of a beta 2-selective adrenoceptor antagonist (ICI 118,551). J. Cardiovasc. Pharmacol. *5*, 430–437.

Black, H.R., Greenberg, B.H., and Weber, M.A. (2010). The foundation role of beta blockers across the cardiovascular disease spectrum: a year 2009 update. Am. J. Med. *123*, S2.

Blaženović, I., Kind, T., Ji, J., and Fiehn, O. (2018). Software Tools and Approaches for Compound Identification of LC-MS/MS Data in Metabolomics. Metabolites *8*, E31.

Brown, J.M., and Hazen, S.L. (2018). Microbial modulation of cardiovascular disease. Nat. Rev. Microbiol. *16*, 171–181.

Brusilow, S., Tinker, J., and Batshaw, M.L. (1980). Amino acid acylation: a mechanism of nitrogen excretion in inborn errors of urea synthesis. Science *207*, 659–661.

Burnett, H., Earley, A., Voors, A.A., Senni, M., McMurray, J.J., Deschaseaux, C., and Cope, S. (2017). Thirty Years of Evidence on the Efficacy of Drug Treatments for Chronic Heart Failure With Reduced Ejection Fraction: A Network Meta-Analysis. Circ Heart Fail *10*, e003529.

Cameron, S.J., Mix, D.S., Ture, S.K., Schmidt, R.A., Mohan, A., Pariser, D., Stoner, M.C., Shah, P., Chen, L., Zhang, H., et al. (2018). Hypoxia and Ischemia Promote a Maladaptive Platelet Phenotype. Arterioscler. Thromb. Vasc. Biol. *38*, 1594–1606.

Campbell, A.P., and Smrcka, A.V. (2018). Targeting G protein-coupled receptor signalling by blocking G proteins. Nat. Rev. Drug Discov. *17*, 789–803.

Ciccarelli, M., Santulli, G., Pascale, V., Trimarco, B., and Iaccarino, G. (2013). Adrenergic receptors and metabolism: role in development of cardiovascular disease. Front. Physiol. *4*, 265.

Colman, R.W. (1990). Platelet receptors. Hematol. Oncol. Clin. North Am. *4*, 27–42.

da Silva, R.R., Dorrestein, P.C., and Quinn, R.A. (2015). Illuminating the dark matter in metabolomics. Proc. Natl. Acad. Sci. USA *112*, 12549–12550.

Devlin, A.S., Marcobal, A., Dodd, D., Nayfach, S., Plummer, N., Meyer, T., Pollard, K.S., Sonnenburg, J.L., and Fischbach, M.A. (2016). Modulation of a Circulating Uremic Solute via Rational Genetic Manipulation of the Gut Microbiota. Cell Host Microbe *20*, 709–715.

Dickert, S., Pierik, A.J., and Buckel, W. (2002). Molecular characterization of phenyllactate dehydratase and its initiator from Clostridium sporogenes. Mol. Microbiol. *44*, 49–60.

Dodd, D., Spitzer, M.H., Van Treuren, W., Merrill, B.D., Hryckowian, A.J., Higginbottom, S.K., Le, A., Cowan, T.M., Nolan, G.P., Fischbach, M.A., and Sonnenburg, J.L. (2017). A gut bacterial pathway metabolizes aromatic amino acids into nine circulating metabolites. Nature *551*, 648–652.

Duckworth, W., Abraira, C., Moritz, T., Reda, D., Emanuele, N., Reaven, P.D., Zieve, F.J., Marks, J., Davis, S.N., Hayward, R., et al.; VADT Investigators (2009). Glucose control and vascular complications in veterans with type 2 diabetes. N. Engl. J. Med. *360*, 129–139.

Elliott, P., Posma, J.M., Chan, Q., Garcia-Perez, I., Wijeyesekera, A., Bictash, M., Ebbels, T.M., Ueshima, H., Zhao, L., van Horn, L., et al. (2015). Urinary metabolic signatures of human adiposity. Sci. Transl. Med. *7*, 285ra62.

Elsden, S.R., Hilton, M.G., and Waller, J.M. (1976). The end products of the metabolism of aromatic amino acids by Clostridia. Arch. Microbiol. *107*, 283–288.

Fawzi, A.B., Macdonald, D., Benbow, L.L., Smith-Torhan, A., Zhang, H., Weig, B.C., Ho, G., Tulshian, D., Linder, M.E., and Graziano, M.P. (2001). SCH-202676: An allosteric modulator of both agonist and antagonist binding to G protein-coupled receptors. Mol. Pharmacol. *59*, 30–37.

Fu, Q., Wang, Q., and Xiang, Y.K. (2017). Insulin and β Adrenergic Receptor Signaling: Crosstalk in Heart. Trends Endocrinol. Metab. *28*, 416–427.

Gerstein, H.C., Mann, J.F., Yi, Q., Zinman, B., Dinneen, S.F., Hoogwerf, B., Hallé, J.P., Young, J., Rashkow, A., Joyce, C., et al.; HOPE Study Investigators (2001). Albuminuria and risk of cardiovascular events, death, and heart failure in diabetic and nondiabetic individuals. JAMA *286*, 421–426.

González-Guardia, L., Yubero-Serrano, E.M., Delgado-Lista, J., Perez-Martinez, P., Garcia-Rios, A., Marin, C., Camargo, A., Delgado-Casado, N., Roche, H.M., Perez-Jimenez, F., et al. (2015). Effects of the Mediterranean diet supplemented with coenzyme q10 on metabolomic profiles in elderly men and women. J. Gerontol. A Biol. Sci. Med. Sci. *70*, 78–84.

Guo, C.J., Allen, B.M., Hiam, K.J., Dodd, D., Van Treuren, W., Higginbottom, S., Nagashima, K., Fischer, C.R., Sonnenburg, J.L., Spitzer, M.H., and Fischbach, M.A. (2019). Depletion of microbiome-derived molecules in the host using *Clostridium* genetics. Science *366*, eaav1282.

Gupta, R., Tang, W.H., and Young, J.B. (2004). Patterns of beta-blocker utilization in patients with chronic heart failure: experience from a specialized outpatient heart failure clinic. Am. Heart J. *147*, 79–83.

Gupta, N., Li, W., and McIntyre, T.M. (2015). Deubiquitinases Modulate Platelet Proteome Ubiquitination, Aggregation, and Thrombosis. Arterioscler. Thromb. Vasc. Biol. *35*, 2657–2666.

Hein, L. (2006). Adrenoceptors and signal transduction in neurons. Cell Tissue Res. *326*, 541–551.

Hein, L., and Kobilka, B.K. (1997). Adrenergic Receptors From Molecular Structure to in vivo function. Trends Cardiovasc. Med. *7*, 137–145.

Ilardi, F., Gargiulo, G., Schiattarella, G.G., Giugliano, G., Paolillo, R., Menafra, G., De Angelis, E., Scudiero, L., Franzone, A., Stabile, E., et al. (2018). Effects of Carvedilol Versus Metoprolol on Platelet Aggregation in Patients With Acute Coronary Syndrome: The PLATE-BLOCK Study. Am. J. Cardiol. *122*, 6–11.

Jonsson, A.L., and Bäckhed, F. (2017). Role of gut microbiota in atherosclerosis. Nat. Rev. Cardiol. *14*, 79–87.

Koeth, R.A., Wang, Z., Levison, B.S., Buffa, J.A., Org, E., Sheehy, B.T., Britt, E.B., Fu, X., Wu, Y., Li, L., et al. (2013). Intestinal microbiota metabolism of L-carnitine, a nutrient in red meat, promotes atherosclerosis. Nat. Med. *19*, 576–585.

Koeth, R.A., Lam-Galvez, B.R., Kirsop, J., Wang, Z., Levison, B.S., Gu, X., Copeland, M.F., Bartlett, D., Cody, D.B., Dai, H.J., et al. (2019). l-Carnitine in omnivorous diets induces an atherogenic gut microbial pathway in humans. J. Clin. Invest. *129*, 373–387.

Koh, A., Molinaro, A., Stahlman, M., Khan, M.T., Schmidt, C., Manneras-Holm, L., Wu, H., Carreras, A., Jeong, H., Olofsson, L.E., et al. (2018). Microbially Produced Imidazole Propionate Impairs Insulin Signaling through mTORC1. Cell *175*, 947–961.e917.

Koopen, A.M., Groen, A.K., and Nieuwdorp, M. (2016). Human microbiome as therapeutic intervention target to reduce cardiovascular disease risk. Curr. Opin. Lipidol. *27*, 615–622.

Koryakina, Y., Jones, S.M., Cornett, L.E., Seely, K., Brents, L., Prather, P.L., Kofman, A., and Kurten, R.C. (2012). Effects of the β-agonist, isoprenaline, on the down-regulation, functional responsiveness and trafficking of β2-adrenergic receptors with N-terminal polymorphisms. Cell Biol. Int. *36*, 1171–1183.

Lefkowitz, R.J., Rockman, H.A., and Koch, W.J. (2000). Catecholamines, cardiac beta-adrenergic receptors, and heart failure. Circulation *101*, 1634–1637.

Leitinger, B. (2011). Transmembrane collagen receptors. Annu. Rev. Cell Dev. Biol. *27*, 265–290.

Lewandowicz, A.M., Vepsäläinen, J., and Laitinen, J.T. (2006). The 'allosteric modulator' SCH-202676 disrupts G protein-coupled receptor function via sulphydryl-sensitive mechanisms. Br. J. Pharmacol. *147*, 422–429.

Li, X.S., Wang, Z., Cajka, T., Buffa, J.A., Nemet, I., Hurd, A.G., Gu, X., Skye, S.M., Roberts, A.B., Wu, Y., et al. (2018). Untargeted metabolomics identifies trimethyllysine, a TMAO-producing nutrient precursor, as a predictor of incident cardiovascular disease risk. JCI Insight *3*, 99096.

Lloyd-Price, J., Arze, C., Ananthakrishnan, A.N., Schirmer, M., Avila-Pacheco, J., Poon, T.W., Andrews, E., Ajami, N.J., Bonham, K.S., Brislawn, C.J., et al.; IBDMDB Investigators (2019). Multi-omics of the gut microbial ecosystem in inflammatory bowel diseases. Nature *569*, 655–662.

Loo, R.L., Zou, X., Appel, L.J., Nicholson, J.K., and Holmes, E. (2018). Characterization of metabolic responses to healthy diets and association with blood pressure: application to the Optimal Macronutrient Intake Trial for Heart Health (OmniHeart), a randomized controlled study. Am. J. Clin. Nutr. *107*, 323–334.

Masureel, M., Zou, Y., Picard, L.P., van der Westhuizen, E., Mahoney, J.P., Rodrigues, J.P.G.L.M., Mildorf, T.J., Dror, R.O., Shaw, D.E., Bouvier, M., et al. (2018). Structural insights into binding specificity, efficacy and bias of a β_2AR partial agonist. Nat. Chem. Biol. *14*, 1059–1066.

Meyer, T.W., Sirich, T.L., Fong, K.D., Plummer, N.S., Shafi, T., Hwang, S., Banerjee, T., Zhu, Y., Powe, N.R., Hai, X., and Hostetter, T.H. (2016). Kt/Vurea and Nonurea Small Solute Levels in the Hemodialysis Study. J. Am. Soc. Nephrol. *27*, 3469–3478.

Milligan, G., and Kostenis, E. (2006). Heterotrimeric G-proteins: a short history. Br. J. Pharmacol. *147* (*Suppl 1*), S46–S55.

Moldave, K., and Meister, A. (1957). Synthesis of phenylacetylglutamine by human tissue. J. Biol. Chem. *229*, 463–476.

Naga Prasad, S.V., Barak, L.S., Rapacciuolo, A., Caron, M.G., and Rockman, H.A. (2001). Agonist-dependent recruitment of phosphoinositide 3-kinase to the membrane by beta-adrenergic receptor kinase 1. A role in receptor sequestration. J. Biol. Chem. *276*, 18953–18959.

O'Rourke, M.F., Blaxall, H.S., Iversen, L.J., and Bylund, D.B. (1994). Characterization of [3H]RX821002 binding to alpha-2 adrenergic receptor subtypes. J. Pharmacol. Exp. Ther. *268*, 1362–1367.

Petrikova, M., Jancinova, V., Nosal, R., Majekova, M., and Fabryova, V. (2005). Carvedilol–a beta-blocker with considerable antiaggregatory effect on human blood platelets. Bratisl. Lek. Listy *106*, 20–25.

Piarulli, F., Sartore, G., Ceriello, A., Ragazzi, E., Reitano, R., Nollino, L., Cosma, C., Fedele, D., and Lapolla, A. (2009). Relationship between glyco-oxidation, antioxidant status and microalbuminuria in type 2 diabetic patients. Diabetologia *52*, 1419–1425.

Pluskal, T., Castillo, S., Villar-Briones, A., and Oresic, M. (2010). MZmine 2: modular framework for processing, visualizing, and analyzing mass spectrometry-based molecular profile data. BMC Bioinformatics *11*, 395.

Poesen, R., Claes, K., Evenepoel, P., de Loor, H., Augustijns, P., Kuypers, D., and Meijers, B. (2016). Microbiota-Derived Phenylacetylglutamine Associates with Overall Mortality and Cardiovascular Disease in Patients with CKD. J. Am. Soc. Nephrol. *27*, 3479–3487.

Rockman, H.A., Koch, W.J., and Lefkowitz, R.J. (2002). Seven-transmembrane-spanning receptors and heart function. Nature *415*, 206–212.

Schmidt, R.A., Morrell, C.N., Ling, F.S., Simlote, P., Fernandez, G., Rich, D.Q., Adler, D., Gervase, J., and Cameron, S.J. (2018). The platelet phenotype in patients with ST-segment elevation myocardial infarction is different from non-ST-segment elevation myocardial infarction. Transl. Res. *195*, 1–12.

Schröder, R., Janssen, N., Schmidt, J., Kebig, A., Merten, N., Hennen, S., Müller, A., Blättermann, S., Mohr-Andrä, M., Zahn, S., et al. (2010). Deconvolution of complex G protein-coupled receptor signaling in live cells using dynamic mass redistribution measurements. Nat. Biotechnol. *28*, 943–949.

Schröder, R., Schmidt, J., Blättermann, S., Peters, L., Janssen, N., Grundmann, M., Seemann, W., Kaufel, D., Merten, N., Drewke, C., et al. (2011). Applying label-free dynamic mass redistribution technology to frame signaling of G protein-coupled receptors noninvasively in living cells. Nat. Protoc. *6*, 1748–1760.

Shafi, T., Meyer, T.W., Hostetter, T.H., Melamed, M.L., Parekh, R.S., Hwang, S., Banerjee, T., Coresh, J., and Powe, N.R. (2015). Free Levels of Selected Organic Solutes and Cardiovascular Morbidity and Mortality in Hemodialysis Patients: Results from the Retained Organic Solutes and Clinical Outcomes (ROSCO) Investigators. PLoS ONE *10*, e0126048.

Shafi, T., Sirich, T.L., Meyer, T.W., Hostetter, T.H., Plummer, N.S., Hwang, S., Melamed, M.L., Banerjee, T., Coresh, J., and Powe, N.R. (2017). Results of the HEMO Study suggest that p-cresol sulfate and indoxyl sulfate are not associated with cardiovascular outcomes. Kidney Int. *92*, 1484–1492.

Skye, S.M., Zhu, W., Romano, K.A., Guo, C.J., Wang, Z., Jia, X., Kirsop, J., Haag, B., Lang, J.M., DiDonato, J.A., et al. (2018). Microbial Transplantation With Human Gut Commensals Containing CutC Is Sufficient to Transmit Enhanced Platelet Reactivity and Thrombosis Potential. Circ. Res. *123*, 1164–1176.

Small, K.M., McGraw, D.W., and Liggett, S.B. (2003). Pharmacology and physiology of human adrenergic receptor polymorphisms. Annu. Rev. Pharmacol. Toxicol. *43*, 381–411.

Srikanthan, S., Li, W., Silverstein, R.L., and McIntyre, T.M. (2014). Exosome poly-ubiquitin inhibits platelet activation, downregulates CD36 and inhibits pro-atherothombotic cellular functions. J. Thromb. Haemost. *12*, 1906–1917.

Tang, W.H., Wang, Z., Levison, B.S., Koeth, R.A., Britt, E.B., Fu, X., Wu, Y., and Hazen, S.L. (2013). Intestinal microbial metabolism of phosphatidylcholine and cardiovascular risk. N. Engl. J. Med. *368*, 1575–1584.

Tsugawa, H., Cajka, T., Kind, T., Ma, Y., Higgins, B., Ikeda, K., Kanazawa, M., VanderGheynst, J., Fiehn, O., and Arita, M. (2015). MS-DIAL: data-independent MS/MS deconvolution for comprehensive metabolome analysis. Nat. Methods *12*, 523–526.

Urpi-Sarda, M., Almanza-Aguilera, E., Llorach, R., Vázquez-Fresno, R., Estruch, R., Corella, D., Sorli, J.V., Carmona, F., Sanchez-Pla, A., Salas-Salvadó, J., and Andres-Lacueva, C. (2019). Non-targeted metabolomic biomarkers and metabotypes of type 2 diabetes: A cross-sectional study of PREDIMED trial participants. Diabetes Metab. *45*, 167–174.

Wang, Z., Nicholls, S.J., Rodriguez, E.R., Kummu, O., Hörkkö, S., Barnard, J., Reynolds, W.F., Topol, E.J., DiDonato, J.A., and Hazen, S.L. (2007). Protein carbamylation links inflammation, smoking, uremia and atherogenesis. Nat. Med. *13*, 1176–1184.

Wang, Z., Klipfell, E., Bennett, B.J., Koeth, R., Levison, B.S., Dugar, B., Feldstein, A.E., Britt, E.B., Fu, X., Chung, Y.M., et al. (2011). Gut flora metabolism of phosphatidylcholine promotes cardiovascular disease. Nature *472*, 57–63.

Wang, L., Tang, Y., Liu, S., Mao, S., Ling, Y., Liu, D., He, X., and Wang, X. (2013). Metabonomic profiling of serum and urine by (1)H NMR-based spectroscopy discriminates patients with chronic obstructive pulmonary disease and healthy individuals. PLoS ONE *8*, e65675.

Watson, L.J., Alexander, K.M., Mohan, M.L., Bowman, A.L., Mangmool, S., Xiao, K., Naga Prasad, S.V., and Rockman, H.A. (2016). Phosphorylation of Src by phosphoinositide 3-kinase regulates beta-adrenergic receptor-mediated EGFR transactivation. Cell. Signal. *28*, 1580–1592.

Webster, L.T., Siddiqui, U.A., Lucas, S.V., Strong, J.M., and Mieyal, J.J. (1976). Identification of separate acyl- CoA:glycine and acyl-CoA:L-glutamine N-acyltransferase activities in mitochondrial fractions from liver of rhesus monkey and man. J. Biol. Chem. *251*, 3352–3358.

Witte, K.K., Drozd, M., Walker, A.M.N., Patel, P.A., Kearney, J.C., Chapman, S., Sapsford, R.J., Gierula, J., Paton, M.F., Lowry, J., et al. (2018). Mortality Reduction Associated With β-Adrenoceptor Inhibition in Chronic Heart Failure Is Greater in Patients With Diabetes. Diabetes Care *41*, 136–142.

Yang, D., Previs, S.F., Fernandez, C.A., Dugelay, S., Soloviev, M.V., Hazey, J.W., Agarwal, K.C., Levine, W.C., David, F., Rinaldo, P., et al. (1996). Noninvasive probing of citric acid cycle intermediates in primate liver with phenylacetylglutamine. Am. J. Physiol. *270*, E882–E889.

Zhang, L., Wei, T.T., Li, Y., Li, J., Fan, Y., Huang, F.Q., Cai, Y.Y., Ma, G., Liu, J.F., Chen, Q.Q., et al. (2018). Functional Metabolomics Characterizes a Key Role for *N*-Acetylneuraminic Acid in Coronary Artery Diseases. Circulation *137*, 1374–1390.

Zhu, W., Gregory, J.C., Org, E., Buffa, J.A., Gupta, N., Wang, Z., Li, L., Fu, X., Wu, Y., Mehrabian, M., et al. (2016). Gut Microbial Metabolite TMAO Enhances Platelet Hyperreactivity and Thrombosis Risk. Cell *165*, 111–124.

STAR★METHODS

KEY RESOURCES TABLE

REAGENT or RESOURCE	SOURCE	IDENTIFIER
Antibodies		
FITC IgM Isotype control	BD PharMingen	Cat#555583; RRID:AB_395959
FITC Mouse Anti-human PAC-1	BD PharMingen	Cat#340507; RRID:AB_2230769
PE IgG isotype control	BD PharMingen	Cat#555749; RRID:AB_396091
PE Mouse Anti-human CD62P (P-selectin)	BD PharMingen	Cat#555524; RRID:AB_395910
Bacterial and Virus Strains		
C. sporogenes	ATCC	Cat#15579
ΔcutC C. sporogenes	Guo et al., 2019	N/A
ΔcutCΔfldH C. sporogenes	This study	N/A
ΔcutCΔporA C. sporogenes	This study	N/A
E. coli CA434 (HB101/pRK24) harboring the pMTL007C-E2	Gift from Justin Sonnenburg Lab (Dodd et al., 2017)	Stanford University
Biological Samples		
Human peripheral plasma	Clinical Trials	N/A
Chemicals, Peptides, and Recombinant Proteins		
Phenylacetylglutamine (PAGln)	Santa Cruz Biotechnology	Cat#SC-212551A
Phenylacetylglycine (PAGly)	Bachem	Cat#4016439.0001
D_5-Phenylacetylglutamine (D_5-PAgln)	CDN Isotopes	Cat#D-6900
Acetonitrile UHPLC-MS	Thermo Fisher Scientific	Cat#A956-1
Water UHPLC-MS	Thermo Fisher Scientific	Cat#W8-1
Isopropanol Optima LC-MS	Fisher Chemicals	Cat#A461-212
Methanol Optima LC-MS	Fisher Chemicals	Cat#A454-4
Ammonium formate Optima LC-MS	Fisher Chemicals	Cat#A115-50
Ammonium acetate Optima LC-MS	Fisher Chemicals	Cat#A114-50
Formic acid Optima LC-MS	Fisher Chemicals	Cat#A117-50
Acetic acid Optima LC-MS	Fisher Chemicals	Cat#A113-50
NaOH	Fisher BioReagents	Cat# BP359-500
Propanol	Fisher BioReagents	Cat# BP1130-500
Pyrdine	Sigma Aldrich	Cat#33553-1L
Propyl chloroformate	Aldrich	Cat#249467-25 g
Hexane HPLC plus	Sigma-Aldrich	Cat#650552-4L
L-$^{13}C_9$-$^{15}N_1$-Phenylalaine	Aldrich	Cat#608017-0.5G
Kanamycin sulfate	GIBCO	Cat#11815-032
Gentamicin sulfate	Gold Biotechnology	Cat#G-400-10
Colistin sulfate	Gold Biotechnology	Cat#C-921-25
Metronidazole	Sigma-Aldrich	Cat#M3761-100
Vancomycin hydrochloride	Chem-Impex Int'l.	Cat#00315
Erythromycin	Teknova	Cat#E5305
Saline	Baxter	Cat#2B1306
Type 1 collagen	Chrono-Log	Cat#385
PBS (10x)	Media Core	Cat#123-1000
Calcein AM	Invitrogen	Cat#C34852
Prostaglandin E1 (PGE-1)	Sigma	Cat#P5515
KCl	MP Biochemical	Cat#194844

(*Continued on next page*)

Continued

REAGENT or RESOURCE	SOURCE	IDENTIFIER
NaCl	Fisher BioReagents	Cat#BP358-212
Na_2HPO_4	Fisher BioReagents	Cat#BP332-500
$MgCl_2$ x $6H_2O$	Fisher BioReagents	Cat#BP214-500
Glucose	Fisher Chemicals	Cat#D16-500
$NaHCO_3$	Sigma	Cat#S-6297
NaH_2PO_4	Fisher BioReagents	Cat#BP329-1
HEPES	Sigma	Cat#H3375-500
TRAP-6	Tocris	Cat#3497
KH_2PO_4	VWR Life Science	Cat#0781-2.5
$CaCl_2$ x $2H_2O$	ACROS	Cat#423525000
$MgSO_4$ x $7H_2O$	Sigma	Cat#M-2773
Fura 2-AM	Invitrogen	Cat#F1201
ADP	Chrono-Log	Cat#384
Thrombin	Sigma	Cat#T1063-50UN
Rhodamine 6G	Sigma	Cat#252433
$FeCl_3$	Sigma	Cat#157740
Glycerol	Fisher Bioreagents	Cat#BP229-1
HBSS (1x)	Media Core LRI	Cat#189Y500CUST
HEPES (1 M; pH 7.4)	Media Core LRI	Cat#389V100CUST
RPMI 1640 media	Media Core LRI	Cat#10-500
opti-MEM media	Media Core LRI	Cat#35-500
DMEM media	Media Core LRI	Cat#99G500CUST
Penicillin-Streptomycin	Media Core LRI	Cat#725-100
Norepinephrine	Sigma	Cat#A0937
Phenylalanine	Sigma-Aldrich	Cat#P5030
Pertussis toxin (PTX)	Tocris	Cat#3097
Cholera toxin (CTX)	Sigma	Cat#C9903
YM-254890	Wako	Cat#257-00631
SCH-202676	Tocris	Cat#1400
Epinephrine	Sigma	Cat#E4642
ATP	Sigma	Cat#A9187
ICI118,551	Tocris	Cat#0821
Isoproterenol (ISO)	Sigma	Cat#I6504
B-HT933	Tocris	Cat#2758
TRIZOL	Invitrogen	Cat#15596026
IBMX	Sigma	Cat#I5879
Rolipram	Tocris	Cat#0905
BSA	Sigma	Cat#A7906
FBS	Gemini Bio-Products	Cat#100-106
Tris Base	Fisher BioReagents	Cat#BP152
EDTA	Sigma	Cat#E5134
Leupeptin	Sigma	Cat#L8511
Aprotinin	Sigma	Cat#A6279
^{125}Iodo-(-)-Cyanopindolol	Perkin Elmer Health Sciences	Cat#NEX189100UC
Propranolol	Sigma	Cat#P0884
TFLLR-NH2	Tocris	Cat#1464
Chloramphenicol	Sigma-Aldrich	Cat# C0378
D-Cycloserine	Sigma-Aldrich	Cat# C3909

(*Continued on next page*)

Continued

REAGENT or RESOURCE	SOURCE	IDENTIFIER
Thiamphenicol	Sigma-Aldrich	Cat# T0261
Critical Commercial Assays		
Ambion- Lipofactamine RNAiMAX	Invitrogen	Cat#13778150
Lipofactamine 3000 Transfection kit	Invitrogen	Cat#L3000008
High-Capacity RNA to cDNA kit	Applied Biosystems	Cat#4387406
CatchPoint Cyclic-AMP Fluorescent Assay Kit	Molecular Devices	Cat#R8089
FLIPR Calcium 5 Assay Kit	Molecular Devices	Cat#R8186
NucleoSpin Tissue kit	Macherey-Nagel	Cat#740952.250
DNeasy Blood and Tissue Kit	QIAGEN	Cat#69504
Experimental Models: Cell Lines		
HEK293	ATCC	Cat#CRL-1573
β2-HEK293 (stable)	Watson et al., 2016	N/A
MEG01	ATCC	Cat#CRL-2021
HEL92.1.7	ATCC	Cat#TIB-180
CHO-K1	ATCC	Cat#CCL-61
Experimental Models: Organisms/Strains		
C57BL/6J	The Jackson Laboratory	Cat#000664
C57BL/6 (re-Derived Germ-Free)	Germ-free mice raised in the gnotobiotic facility at the University of Wisconsin – Madison or University of Nebraska-Lincoln	N/A
Oligonucleotides		
pcDNA3.1(+)-N-DYK vector	Genescript	Cat#SC1317
pcDNA3.1(+)-ADRA2A-N-DYK	This study, Addgene	Cat#139514
pcDNA3.1(+)-ADRA2B-N-DYK	This study, Addgene	Cat#139515
pcDNA3.1(+)-ADRB2-N-DYK	This study, Addgene	Cat#139516
Silencer select ADRA2A siRNA	Thermo Fisher Scientific	Assay ID s1112 Cat#4427037
Silencer select ADRA2A siRNA	Thermo Fisher Scientific	Assay ID s1113 Cat#4427037
Silencer select ADRA2A siRNA	Thermo Fisher Scientific	Assay ID s1114 Cat#4427037
Silencer select ADRA2B siRNA	Thermo Fisher Scientific	Assay ID s1115 Cat#4427037
Silencer select ADRA2B siRNA	Thermo Fisher Scientific	Assay ID s1116 Cat#4427037
Silencer select ADRA2B siRNA	Thermo Fisher Scientific	Assay ID s1117 Cat#4427037
Silencer select ADRB2 siRNA	Thermo Fisher Scientific	Assay ID s1121 Cat#4427037
Silencer select ADRB2 siRNA	Thermo Fisher Scientific	Assay ID: s1122 Cat#4427037
Silencer select ADRB2 siRNA	Thermo Fisher Scientific	Assay ID: s1123 Cat#4427037
Silencer select Scrambled siRNAs (Negative control No 1)	Thermo Fisher Scientific	Cat#4390843
Silencer select Scrambled siRNAs (Negative control No 2)	Thermo Fisher Scientific	Cat#4390846
Software and Algorithms		
MZmine 2	Pluskal et al., 2010	N/A
MultiQuant	Sciex	N/A
Prism (version 8)	GraphPad	N/A
Lab Solutions	Shimadzu Scientific Instruments	N/A
R Version 3.5.1.		https://www.r-project.org
Other		
UPLC ACQUITY BEH Amide column (150 × 2.1 mm; 1.7 μm)	Waters	Cat#186004802
UPLC BEH Amide VanGuard precolumn (5 × 2.1 mm; 1.7 μm)	Waters	Cat#186007760
UPLC XBridge BEH Amide column (150 × 2.1 mm; 2.5 μm)	Waters	Cat#186006724
Agilent 1290 Infinity LC system	Agilent	N/A

(*Continued on next page*)

Continued

REAGENT or RESOURCE	SOURCE	IDENTIFIER
TripleTOF 5600+	Sciex	N/A
Glass fiber	Brandel	Cat#FP-205
Membrane harvester	Brandel	N/A
Gamma counter	ICN Biomedicals	N/A
Kinetex C18 column (50 mm × 2.1 mm; 2.6 μm)	Phenomenex	Cat#00B-4462-AN
SecurityGuard ULTRA Cartridges – UHPLC C18 2.1 mm	Phenomenex	Cat#AJ0-8782
2 LC-20AD Shimadazu pump system	Shimadzu Scientific Instruments	NA
SIL-HTC autosampler	Shimadzu Scientific Instruments	N/A
Strata C18_E (55 μm, 70 A; 20 g/60 mL Giga Tubes)	Phenomenex	Cat#8B-S001-VFF
Amicon Ultra −0.5 mL Centrifuge Filters; Ultracel 3K	Merck Millipore	Cat#UFC500396
Semipreparative C18 column; ODS, 10x250 mm; 5 μm	Beckman Coulter	Cat#235328
Shimadzu LC-30 AD pumps (Nexera X2), a CTO 20AC oven operating at 30°C, and a SIL-30 AC-MP	Shimadzu Scientific Instruments	N/A
Triple quadruple mass spectrometer from 8050 series	Shimadzu Scientific Instruments	N/A
Cellix Microfluidics System	Cellix	N/A
Leica DMI6000 inverted microscope equipped with an environmental chamber and cooled CCD camera	Leica	N/A
Vena8 Fluoro+ biochip	Cellix	Cat#V8CF-400-100-02P10
Hemocytometer	Hausser Scientific	N/A
Spectrofluorometer	Photon Technology International	N/A
FlexStation 3 Multi-Mode Microplate Reader	Molecular Devices	N/A
Intravital fluorescence microscopy equipped with video recording	Leica	N/A
Culture media plates	Anaerobe Systems	Cat#AS-141
DMR Epic BT 5053	Corning	N/A
Fibronectin coated epic corning DMR plate	Corning	Cat#5082
Black wall cell culture plates	Corning	Cat#353219

LEAD CONTACT AND MATERIALS AVAILABILITY

Further information and requests for resources and reagents should be directed to and will be fulfilled by the Lead Contact, Stanley L. Hazen (hazens@ccf.org). All unique/stable reagents generated in this study are available from the Lead Contact with a completed Materials Transfer Agreement. Plasmids generated in this study have been deposited to Addgene pcDNA3.1(+)-ADRA2A-N-DYK, pcDNA3.1(+)-ADRA2B-N-DYK and pcDNA3.1(+)-ADRB2-N-DYK (Cat# 139514, 139515 and 139516, respectively).

EXPERIMENTAL MODEL AND SUBJECT DETAILS

Human Subjects

All subjects gave written informed consent and the Institutional Review Board of the Cleveland Clinic approved all study protocols. The Discovery Cohort (n = 1,157) employed for untargeted metabolomics investigations, and the independent non-overlapping Validation Cohort (n = 4,000), were obtained from sequential consenting subjects enrolled in the study GeneBank at the Cleveland Clinic. GeneBank is a large (n > 10,000) and well-characterized single center cohort with associated tissue repository and longitudinal follow-up clinical database. GeneBank included sequential stable subjects undergoing elective diagnostic coronary evaluations. All subjects underwent elective diagnostic coronary angiography (cardiac catheterization or coronary computed tomography) for evaluation of CAD (Tang et al., 2013; Wang et al., 2011; Wang et al., 2007). All subjects had extensive clinical and longitudinal outcome data monitored, including adjudicated outcomes over the ensuing 3 to 5 years after enrollment. MACE (Major Adverse Cardiovascular Event) was defined as death, nonfatal myocardial infarction, or nonfatal cerebrovascular accident (stroke) following enrollment. High-sensitivity C-reactive protein, and lipid profiles were measured on the Roche Cobas platform (Roche Diagnostics).

Normal range levels of PAGln and PAGly were determined from plasma recovered from a random subset (n = 25) of consenting non-fasting subjects undergoing community health screens. Subjects had no medical history of cardiovascular or metabolic diseases, normal vital signs and screening laboratory results (lipid profile, basic chemistry), and were not on any medications. Human

blood for preparing platelet rich plasma and washed platelet isolation was obtained from healthy consenting donors. In additional studies, healthy volunteers (n = 15) were consented and subjected to a cocktail of oral antibiotics for 7 days (either ciprofloxacin, metronidazole and vancomycin; or ciprofloxacin, metronidazole, vancomycin and neomycin), as previously described (Tang et al., 2013). Volunteers were not pregnant nor had a chronic illness (including a known history of heart failure, renal failure, pulmonary disease, gastrointestinal disorders, or hematologic diseases). Blood was collected after overnight fasting at 3 different time points: at base line (before antibiotics treatment (pre-Abx); right after the 7 day antibiotics regiment (Abx), and after an antibiotics washout period (minimum three weeks) to permit repopulation of normal gut microorganisms (Post-Abx).

Mice

C57BL/6J mice, 8-10 weeks old, were purchased from The Jackson Laboratory and maintained in our facilities. In addition to germ free mice raised in the Cleveland Clinic Lerner Research Institute Gnotobiotic Facility, some of the studies employed germ-free C57BL/6 male mice (8-10 weeks old) that were raised at the University of Wisconsin-Madison or University of Nebraska-Lincoln gnotobiotic animal facilities and shipped germ free to the Cleveland Clinic Lerner Research Institute Gnotobiotic Facility. All gnotobiotic mice were housed in controlled environments in plastic flexible film gnotobiotic isolators with HEPA filters under a strict 14 h light/10 h dark cycle, and with access to sterilized water and food *ad libitum*. Animal care and experimentation were consistent with NIH guidelines and all animal model studies were approved by the Institutional Animal Care and Use Committee at the Cleveland Clinic.

Microorganisms

Clostridium sporogenes (ATCC, 15579) was routinely cultured in TYG (3% w/v tryptone, 2% w/v yeast extract, 0.1% w/v sodium thioglycolate) broth at 37 °C in an anaerobic chamber from Coy Laboratories in an atmosphere of 5% H_2, 10% CO_2 and 85% N_2. The cells were stored as anaerobically prepared 25% v/v glycerol stocks sealed in 12 × 32 mm glass crimp top vials to ensure anoxic conditions during long-term storage. All manipulations with *C. sporogenes* were performed in the anaerobic chamber and with medium and reagents pre-reduced for at least 48 h. The *Escherichia coli* CA434 (HB101/pRK24) conjugation host was routinely cultured at 30 °C in LB broth supplemented with tetracycline (12 μg/mL) to ensure maintenance of the pRK24 plasmid. *E. coli* TG1 was used for routine cloning. Chloramphenicol (25 μg/mL) was used for selection of pMTL007C-E2 plasmids in *E. coli*. HMP reference strains were obtained from the BEI Resources and were cultured in reinforced clostridial medium (RCM) modified to exclude agar and prevent interference with downstream assays. A mutant lacking the *cutC* gene (Guo et al., 2019) was used for the second gene (*fldH* or *porA* disruption). The second gene was disrupted using the ClosTron mutagenesis system, as previously described (Dodd et al., 2017). *E. coli* CA434 (HB101/pRK24) harboring the pMTL007C-E2 with the specific sites retargeting *fldH* (CLOSPO_00316) or *porA* (CLOSPO_00147) were kindly provided from Justin Sonnenburg Lab. To introduce plasmid DNA into *C. sporogenes*, we performed bi-parental mating using a custom filter-mating-based approach. First 1 ml of overnight culture (24–30 h) of these *E. coli* transformants were harvested and washed with sterile phosphate-buffered saline (PBS) to remove residual antibiotics. The cell pellet was re-suspended with 200 μL of an overnight culture in TYG broth (~18 h) of *C. sporogenes cutC* mutant and was incubated anaerobically at 37 °C on TYG agar plates without antibiotics. After 2 days, the cells was collected by scraper and re-suspended with 300 μL of PBS. The cell suspension was plated on TYG agar plates supplemented with D-cylcoserine (250 μg/mL) and thiamphenicol (15 μg/mL) and incubated anaerobically at 37 °C for a few days. Antibiotic resistant colonies were picked and re-streaked on agar plates containing the same antibiotics. Individual well-isolated colonies were then picked and inoculated into TYG broth containing the same antibiotics and glycerol stocks were prepared. Colonies verified by PCR to contain the plasmid of interest were cultured anaerobically in TYG with D-cylcoserine and thiamphenicol, then 100 μL of undiluted, 10-fold diluted or 100-fold diluted cultures were spread onto TYG agar plates supplemented with erythromycin (5 μg/mL). The antibiotic resistant colonies were picked, re-streaked onto TYG agar plates supplemented with erythromycin and well-isolated colonies were inoculated into TYG broth supplemented with erythromycin. Genomic DNA was isolated from candidate clones using the DNeasy Blood and Tissue Kit from QIAGEN and this DNA was used as a template in a PCR using the gene-specific primers. Primer sets were designed to produce a ~600-bp product for the wild-type and ~2,800-bp product for the mutant containing the intron. When verified mutants were streaked onto TYG plates containing thiamphenicol, no growth was observed, indicating that the loss of the pMTL007C-E2 plasmid had occurred. Germ-free, C57BL/6 (male, 8-10-weeks-old), mice were mono-colonized by oral gavage with *C. sporogenes* mutants as described below in METHOD DETAILS.

Cell Lines

Bone marrow derived cell lines, MEG-01 (ATCC, CRL-2021) and HEL92.1.7 (ATCC, TIB-180) were grown in RPMI 1640 media and kept at 37°C in 5% carbon dioxide (CO_2) incubator. Chinese hamster ovary (CHO)-K1 cells (ATCC, CCL-61) and human embryonic kidney (HEK293) cells (ATCC, CRL-1573) were cultured in DMEM media and kept in a 5% CO_2 incubator at 37°C. ADRA2B-HEK293 cells were stably transfected with pcDNA3.1(+)-ADRA2B-N-DYK and G418-resistant cell pool expanded after being selected with G418 (1.5 mg/mL). Unless otherwise stated, all culture media were supplemented with fetal bovine serum (FBS; 10%), penicillin (100 U/mL) and streptomycin (100 μg/mL). β2-HEK293 were cultured as previously described (Watson et al., 2016). Before use, all cell lines used were tested to confirm negative status for mycoplasma (CC cell culture facility).

Plasmids

Mammalian expression plasmids for transfection were made from the human *ADRA2A*, *ADRA2B*, and *ADRB2* cDNA sequences which were synthesized by Genscript (Piscataway, NJ) to lack their initiating methionine (ATG) but to include an amino terminal encoded GGS linker and these ORFs were cloned in-frame behind the DYK (FLAG) epitope in pcDNA3.1(+)-N-DYK to create pcDNA3.1(+)-ADRA2A-N-DYK, pcDNA3.1(+)-ADRA2B-N-DYK and pcDNA3.1(+)-ADRB2-N-DYK respectively. The vector pcDNA3.1(+)-N-DYK was from Genscript (Piscataway, NJ).

Platelet Rich Plasma and Washed Platelet Isolation from Consenting Human Donors

Platelet rich plasma (PRP) was prepared as previously described (Zhu et al., 2016). Whole blood was collected from consenting healthy donors using sodium citrate (0.109 M) as anticoagulant. PRP was isolated by centrifuging at 100 x *g* for 10 min at 22°C. Platelet poor plasma (PPP) was prepared by further centrifugation of remaining blood at 11,000 x *g* for 2 min. Platelets were counted using a hemocytometer and for aggregometry assays, concentrations were adjusted to $2x10^8$/mL with PPP. To prepare washed platelets for intracellular Ca^{2+} measurements, 100 nM prostaglandin E1 (PGE-1) was added to PRP and the PRP was then centrifuged at 500 x *g* for 20 min at 22°C. The platelet pellet was gently washed with a modified phosphate buffer saline (NaCl (137 mM), KCl (2.7 mM), Na_2HPO_4 (12 mM), $MgCl_2$ (1 mM), and glucose (5.5 mM), pH 7.4) with PGE-1 (100 nM), and centrifuged again at 500 x *g* for 20 min. Platelet pellet was then re-suspended in modified Hank's buffered salt solution (HBSS-BSA-glucose; NaCl (0.137 M), KCl (5.4 mM), Na_2HPO_4 (0.25 mM KH_2PO_4 (0.44 mM), $CaCl_2$ (1.3 mM), $MgSO_4$ (1.0 mM), $NaHCO_3$ (4.2 mM), glucose (5 mM) and BSA (0.1%)) with 100 nM PGE-1. For ratiometric fluorescence measurements, washed platelets were incubated with Fura 2-AM (1 μM) at 22°C for 30 min. Excess Fura 2-AM was removed by centrifugation at 500 x *g* for 30 min. Platelet pellet was then re-suspended in modified Hank's buffered salt solution.

METHOD DETAILS

Untargeted LC–MS/MS Analysis of Human Plasma Samples

Untargeted analysis of plasma samples was similar to that described previously (Tsugawa et al., 2015) but with minor modifications. Polar metabolites were extracted from a plasma sample (30 μL) following protein precipitation using an acetonitrile/isopropanol/water (3:3:2, v/v/v) mixture (1 mL). Aliquots (300 μL) were evaporated, resuspended using an acetonitrile/water (4:1, v/v) mixture (60 μL) containing a series of deuterated internal standards, vortexed, centrifuged, and 50 μL supernatant was transferred to a glass *vial* with a microinsert. Hydrophilic interaction chromatography (HILIC) analysis was performed on a system including an Agilent 1290 Infinity LC system (Agilent Technologies) with a pump (G4220A), a column oven (G1316C), an autosampler (G4226A), and a TripleTOF 5600+ (SCIEX). Extracts were separated on an Acquity UPLC BEH Amide column (150 × 2.1 mm; 1.7 μm, Waters) coupled to a Waters Acquity UPLC BEH Amide VanGuard precolumn (5 × 2.1 mm; 1.7 μm). The column was maintained at 45°C at a flow rate of 0.4 mL/min. The mobile phases consisted of (A) water with ammonium formate (10 mM) and formic acid (0.125%) and (B) 95:5 (v/v) acetonitrile/water with ammonium formate (10 mM) and formic acid (0.125%). The separation was conducted using the following gradient: 0 min 100% B; 0–2 min 100% B; 2–7.7 min 70% B; 7.7–9.5 min 40% B; 9.5–10.25 min 30% B; 10.25–12.75 min 100% B; 12.75–17.75 min 100% B. A sample volume of 1 μL was used for the injection. Sample temperature was maintained at 4°C. The QTOF-MS instrument was operated with electrospray ionization in positive ion mode with the following parameters: curtain gas, 35 psi; ion source gas 1, 50 psi; ion source gas 2, 50 psi; temperature, 300°C; ion spray voltage floating, 4.5 kV; declustering potential, 100 V; acquisition speed, 2 spectra/s. For data processing MZmine 2 (Pluskal et al., 2010) and MultiQuant (SCIEX) software programs were used.

Compound Identification

To chemically define the structures of the plasma analyte with *m/z* 265.1188 as PAGln, several approaches were used. PAGln in plasma was identified by HPLC/high-resolution mass spectrometry by demonstrating the same retention time, and high-resolution mass spectrum as authentic standard. Plasma supernatant after protein precipitation with methanol (1:4; v/v) was analyzed by injection onto a C18 column or HILIC column using a 2 LC-20AD Shimadazu pump system with SIL-HTC autosampler interfaced (Shimadzu Scientific Instruments, Columbia, MD, USA) in tandem with a TripleTOF 5600 mass spectrometer (AB SCIEX). Separation was performed by employing the following gradients: For reverse phase chromatographic Kinetex C18 column (50 mm × 2.1 mm; 2.6 μm) (Cat # 00B-4462-AN, Phenomenex, Torrance, CA) was used. Solvent A (0.1% acetic acid in water) and B (0.1% acetic acid in acetonitrile) were run under the following gradient: 0.0 min (0% B); 0.0-2.0 min (0% B); 2.0-5.0 min (0%B→20%B); 5.0-6.0 min (20%B→60%B); 6.0-7.5 min (60%B→70%B); 7.5-8.0 min (70%B→100%B); 8.0-9.5 min (100%); 9.5-10 min (100%B→0%B); 10.0-15.0 min (0% B) with flow rate of 0.4 mL/min and the injection volume of 1 μL. For separation on HILIC column BEH amide column (Bridge column; BEH amide 2.1 × 150 mm x 2.5 μm column) (Cat# 186006724, Waters, Ireland) was used. Solvent A (10 mM ammonium acetate + 0.125% acetic acid in water) and B (10 mM ammonium acetate + 0.125% acetic acid in 95% acetonitrile and 5% water) were run under the following gradient: 0.0 min (100%); 0.0-0.5 min (100% B→70% B); 0.5-1.0 min (70% B→60% B); 1.0-2.0 min (60% B); 2.0-7.0 min (60% B→50% B); 7.0-8.0 min (50% B); 8.0-9.0 min (50% B → 100% B); 9.0-14.0 min (100%). The flow rate was 0.2 mL/min from 0.0-9.0 min and 0.4 mL/min 9.5-14 min. To further confirm the compound's structure, the analyte with *m/z* 265.1188 was first purified from human plasma using the following procedures. Proteins from human plasma (500 mL) were precipitated with ice-cold methanol (1:4; v/v), and supernatant was dried under reduced pressure. The dry residue was dissolved in water

with 0.1% acetic acid (50 mL) and subjected to solid phase extraction on C18 cartridges (Strata C18_E (55 μm, 70 A; 20 g/60 mL Giga Tubes, Phenomenex, Cat# 8B-S001-VFF). Eluted fractions were analyzed by LC-MS/MS and peak fractions containing the compound (with *m/z* 265.1188 and the appropriate retention time) were pooled and dried under reduced pressure. The dried residue was further purified on a semi-preparative C18 column (ODS, 10x250 mm; 5 μm) (Beckman Coulter) by HPLC. The mobile phases consisted of solvents A (0.2% acetic acid in water) and B (0.2% acetic acid in 90% methanol in water) under the following gradient: 0-23 min (0% B→80% B); 23-37 min (80% B → 100% B); 27-32 min (100% B). Fractions were collected every 0.5 min. Fractions containing the compound with *m/z* 265.1188 were dried under reduced pressure and the residue was dissolved in a water solution of NaOH (5.0 mL, 5 mM). In parallel, authentic PAGln standard was similarly resuspended in NaOH (5 mM) and both the semi-purified plasma analyte with *m/z* 265.1188 and the authentic PAGln standard were derivatized separately and analyzed as follows. An aliquot (300 μL) of the purified plasma sample or PAGln NaOH solution was transferred to a glass tube and mixture of propanol/pyridine (3:2, v/v, 300 μL) and propyl chloroformate (50 μL) was added to the samples, and the tubes were capped, vortexed (1 min), and sonicated (2 min). Hexane (300 μL) was added, and liquid/liquid extraction was performed by vortexing the samples for 5 min. The samples were centrifuged (20 min, 5000 x *g*), and the organic layer was transferred to another glass tube and dried under stream of nitrogen. Dry residue was dissolved in 50% methanol in water and subjected to LC-MS analysis on C18 column as described above.

Targeted LC-MS/MS Analysis of Human Plasma Samples

Stable-isotope-dilution LC-MS/MS was used for quantification of PAGln in human (20 μL) plasma. Ice cold methanol containing internal standard (D_5-phenylacetylglutamine) was added to plasma samples (80 μL), followed by vortexing and centrifuging (21,000 x *g*; 4°C for 15 min). The clear supernatant was transferred to glass vials with microinserts and LC-MS/MS analysis was performed on a chromatographic system consisting of two Shimadzu LC-30 AD pumps (Nexera X2), a CTO 20AC oven operating at 30°C, and a SIL-30 AC-MP autosampler in tandem with 8050 triple quadruple mass spectrometer (Shimadzu Scientific Instruments, Columbia, MD, USA). For chromatographic separation, a Kinetex C18 column (50 mm × 2.1 mm; 2.6 μm) (Cat # 00B-4462-AN, Phenomenex, Torrance, CA) was used. Solvent A (0.1% acetic acid in water) and B (0.1% acetic acid in acetonitrile) were run using the following gradient: 0.0 min (0% B); 0.0-2.0 min (0% B); 2.0-5.0 min (0%B→20%B); 5.0-6.0 min (20%B→60%B); 6.0-7.5 min (60% B→70%B); 7.5-8.0 min (70%B→100%B); 8.0-9.5 min (100%); 9.5-10 min (100%B→0%B); 10.0-15.0 min (0% B) with a flow rate of 0.4 mL/min and a 1 μL injection volume. Electrospray ionization in positive mode with multiple reaction monitoring (MRM) was used with the following transitions: *m/z* 265.2→130.15 for PAGln and D5-PAGln *m/z* 270.1→130.15. The following ion source parameters were applied: nebulizing gas flow, 3 L/min; heating gas flow, 10 L/min; interface temperature, 300°C; desolvation line temperature, 250°C; heat block temperature, 400°C; and drying gas flow, 10 L/min. The limit of detection (LOD; 3:1 signal to noise cutoff) and limit of quantification (LOQ; 10:1 signal to noise cutoff) were 0.010 and 0.033 μM, respectively. Quality control samples were run with each batch of samples and inter-batch variations expressed as coefficient of variation (CV) were less than 10%. For data analysis software Lab Solution (Shimadzu) was used.

In Vitro Screening of Phenylacetic Acid and Phenylpropionic Acid Production from Phenylalanine by *C. sporogenes* Mutants

C. sporogenes mutants were grown on tryptic soy blood agar plates (TSBA; Anaerobe Systems, Cat# AS-542) anaerobically for 48 to 72 h at 37°C. Single colonies were then inoculated into Mega Medium (3 mL) and grown anaerobically overnight at 37°C. Overnight culture (100 μL) was added to fresh Mega Medium (1 mL) containing [$^{13}C_9$,^{15}N]-Phe (100 μM) and cultured an additional 24 h. Cultured media was centrifuged and the supernatant was passed through 3K centrifugal filters (Amicon Ultra-0.5 mL Centrifuge filters, Ultracel-3K, Merck Millipore). Filtrate (20 μL) was subjected to stable-isotope-dilution LC-MS/MS analysis for quantification of [$^{13}C_8$]-phenylacetic acid and [$^{13}C_9$]-phenylpropionic acid. Ice cold methanol containing internal standard ([$^{13}C_2$]- phenylacetic acid; 80 μL) was added to the supernatant, followed by vortexing and centrifuging (21,000 x *g*; 4°C for 15 min). The clear supernatant was transferred to glass vials with microinserts. LC-MS/MS analysis was performed on a chromatographic system composed of two Shimadzu LC-30 AD pumps (Nexera X2), a CTO 20AC oven operating at 30°C, and a SIL-30 AC-MP autosampler in tandem with 8050 triple quadruple mass spectrometer (Shimadzu Scientific Instruments, Columbia, MD, USA). For chromatographic separation, a Kinetex C18 column (50 mm × 2.1 mm; 2.6 μm) (Cat # 00B-4462-AN, Phenomenex, Torrance, CA) was used. Solvent A (0.1% acetic acid in water) and B (0.1% acetic acid in acetonitrile) were run using the following gradient: 0.0 min(0% B); 0.0-2.0 min (0% B); 2.0-5.0 min (0%B→20%B); 5.0-6.0 min (20%B→60%B); 6.0-7.5 min (60%B→70%B); 7.5-8.0 min (70%B→100%B); 8.0-9.5 min (100%); 9.5-10 min (100%B→0%B); 10.0-15.0 min (0% B) with flow rate of 0.4 mL/min and the injection volume of 1 μL. Electrospray ionization in the negative ion mode was used with multiple reaction monitoring (MRM) using the following transitions: *m/z* 135.0→91.0 for phenylacetic acid; *m/z* 143.0→ 98.0 for [$^{13}C_8$]- phenylacetic acid; *m/z* 149.50→105 and *m/z* 158→113.0 for phenylpropionic and [$^{13}C_9$]-phenylpropionic acid, respectively and *m/z* 137.0→92.0 for [$^{13}C_2$]- phenylacetic acid (internal standard).

Murine Antibiotic Challenge

C57BL/6J males (n = 11) and females (n = 15) 8-10 weeks old were treated with an antibiotic cocktail to suppress gut-microbial growth, as previously described (Devlin et al., 2016). Whole blood was collected via saphenous vein (survival collection) into heparin treated capillary tubes for base line measurements from mice on regular chow diet. After the baseline collection, mice were given an antibiotic cocktail in their drinking water consisting of kanamycin (0.4 mg/mL), gentamycin (0.035 mg/mL), colistin (0.057 mg/mL),

metronidazole (0.215 mg/mL), vancomycin (0.045 mg/mL), and erythromycin (0.01 mg/mL). The antibiotic cocktail was administered for a total of 5 days, and then a second blood collection was performed. After that mice were put back on regular water without antibiotics. To facilitate microbial recolonization, fecal pellets from conventionally reared littermates, never treated with antibiotics, were added to the cage bedding. Third blood collection was performed 7 days after the antibiotics withdrawal.

Whole Blood *In Vitro* Thrombosis Assay

Microfluidic shear flow experiments were performed using the Cellix Microfluidics System (Cellix, Dublin, Ireland). Where indicated, each micro channel of a Vena8 Fluoro+ biochip was coated with type 1 collagen (15 μL; 150 μg/mL) and placed in a humidified box overnight at 4°C. Before use each channel of the Vena8Fluoro+ biochip was washed with 1X PBS using the Mirus Nanopump. Images were collected using an HC Plan Apo 20X/0.7NA lens on a Leica DMI6000 inverted microscope equipped with an environmental chamber and a Hamamatsu ImagEM cooled CCD camera. Whole blood collected from consented healthy volunteers was fluorescently tagged with Calcein AM and was pretreated with PAGln (10 μM or 100 μM, pH 7.4) or normal saline (control) for 30 min at 22°C. After the incubation, blood was then perfused over chips coated with or without immobilized type 1 collagen (150 μg/mL) at a physiological shear rate (67.5 dynes/cm^2) using a multi-channel microfluidic device for 3 min. Images of fluorescent platelets adhering to the collagen coating were captured every 5 s during that time. In experiments with P-selectin staining, whole blood pretreated with PAGln or saline was stained with phycoerythrin (PE) conjugated anti-P-selectin (CD62P) antibody for 10 min before perfusion over the collagen coated chip at physiological shear rates. At the end of the experiment, the tube containing the whole blood was removed and the 1X PBS in the biochip reservoir was drawn through the channel at 20 dynes/cm^2. Ten images were captured along the length of the channel during that time. Platelet activation and adherence to the collagen surface was then quantified with computer assisted tomographic analyses as previously described (Gupta et al., 2015; Srikanthan et al., 2014). Briefly, images of P-selectin and calcein AM stained thrombi were quantified using Image Pro plus software (Media Cybernetics, Rockville, Maryland, USA). Intensity threshold was chosen to select for specific staining and quantified for integrated optical density (IOD, Area X Intensity).

Aggregometry Assay in Human Platelets Rich Plasma

Aggregometry assays were performed as previously described (Zhu et al., 2016). Whole blood was collected from consenting healthy donors using sodium citrate (0.109 M) as anticoagulant and PRPs were prepared as described above. Platelets were counted using a hemocytometer and concentration was adjusted to 2x10^8/mL with platelet poor plasma. PRPs were then pre-incubated with PAGln or PAGly (100 μM or at indicated concentrations) or vehicle for 30 min at 22°C. After 30 min of pre-incubation PRPs were maintained in suspension with constant stirring (600 rpm) at 37°C and platelet aggregation was initiated using ADP (up to 4 μM) or TRAP6 (up to 10 μM) or collagen (up to 1.0 μg/mL).

Intracellular Ca^{2+} Measurements

Washed platelets from whole blood were prepared and loaded with the ratiometeric calcium sensing dye, Fura-2, as described above. Platelet pellet, after Fura-2 loading, was re-suspended in modified Hank's buffered salt solution and was pre-incubated with PAGln or PAGly (100 μM or at the indicated concentrations) or vehicle for 30 min at 22°C. After the 30 min pre-incubation, intracellular calcium release from washed platelets was induced by suboptimal concentration of thrombin (0.02U) and changes in $[Ca2^+]_i$ was monitored by measuring Fura 2-AM fluorescence using 340/380 nm dual-wavelength excitation and an emission of 510 nm. Studies were performed at 37°C with constant stirring in a temperature controlled spectrofluorometer (Zhu et al., 2016).

Platelet Flow Cytometry Assay

Washed platelets and antibody staining for flow cytometry was performed as described previously with slight modification (Cameron et al., 2018; Schmidt et al., 2018). Whole blood was collected from consenting healthy donors using sodium citrate (0.109 M) as anticoagulant. PRPs were separated by centrifuging at 100 x *g* for 10 min at 22°C. PRPs were then re-suspended in modified Hank's buffered salt solution (HBSS-BSA-glucose; NaCl (0.137 M), KCl (5.4 mM), Na_2HPO_4 (0.25 mM), KH_2PO_4 (0.44 mM) $CaCl_2$ (1.3 mM), $MgSO_4$ (1.0 mM), $NaHCO_3$ (4.2 mM), glucose (5 mM) and BSA (0.1%)) with PGE-1 (100 nM). Washed platelets were separated by centrifugation at 500 x *g* for 10 min and re-suspended in modified Hank's buffered salt solution without PGE1. Final platelet suspensions (100 μL; 2x10^8 platelets/mL) were then pre-incubated with PAGln (100 μM or at indicated concentration) for 30 min at 22°C before stimulation with 2 μM ADP for 10 min. PE conjugated anti-P-selectin (CD62P-PE; 1 μL) or Fluorescein isothiocyanate (FITC) conjugated PAC1 (binds only to active conformation of GP IIb/IIIa) or isotype control antibody was added to each tube and incubated in the dark for 20 min (to avoid photo bleaching). The platelet suspensions were then fixed with 100 μL of 2% paraformaldehyde. Data was acquired on a flow cytometer (FACS LSRFortessa, BD Biosciences). The instrument was set up and standardized using BD Cytometer Setup and Tracking (CS&T) procedures according to manufacturer specifications. Twenty thousand (20,000) events were acquired. The data was analyzed using FlowJo v10 software. The washed platelets were gated to exclude doublets and the raw mean fluorescent intensity (MFI) of either P-selectin (CD62P) or PAC-1 was generated.

Gnotobiotic Mouse Colonization

C. sporogenes mutants were grown on tryptic soy blood agar plates (TSBA; Anaerobe Systems, Cat# AS-542) anaerobically for 48 to 72 h at 37°C. Single colonies were picked and used to inoculate Mega Medium (3 mL) in prepared Hungate Tubes. Cultures were

grown anaerobically for 18-24 h at 37°C. At that time an aliquot of culture (500 μL) was removed and the remaining bacterial culture was diluted 1:1 with glycerol (40%) in water (v:v) and stored at −80°C. The aliquot was centrifuged and supernatant screened on the LC/MS for metabolite profile while DNA was isolated from the pellet for both 16 s rRNA gene sequencing (described below) and PCR confirmation of presence/absence of *porA* or *fldH*. Germ-free, C57BL/6, male, 8-10-week-old mice were mono-colonized by oral gavage with ~0.2 mL of bacterial culture inside the biological safety cabinet, using the indicated *C. sporogenes* mutants. Mice were maintained on a sterilized diet, and 24 h prior to *in vivo* thrombosis, were injected with filtered sterilized folic acid (250 mg/kg). At the time of sacrifice (2-7 days post colonization), mice were subjected to carotid artery $FeCl_3$ injury thrombosis assay and tissues were collected immediately after the assay, frozen, and stored at −80°C. Following colonization, the investigator was not blinded from treatment groups to avoid cross contamination. To confirm colonization DNA was isolated from flash frozen cecal contents of colonized mice with the NucleoSpin Tissue kit (Macherey-Nagel) according to manufacturer's instructions for bacterial DNA isolation. Isolated DNA was used in a PCR reaction with GoTaq Green Master Mix and the 8F and 1492R 16S rRNA universal primers. PCR reactions were carried out in a 96 well plate with 20 μl final reaction volumes as follows: 95°C for 2 min; 95°C for 30 s, 51°C for 30 s, 72°C for 1 min and 20 s (x30); 72°C for 5 min. Completed reactions were sent to Eurofins Genomics for PCR cleanup and 16S rRNA gene sequencing using their standard house primers (16F). Sequence identity was confirmed using NCBI BLAST.

Carotid Artery $FeCl_3$ Injury Thrombosis Assay

Monocolonized or *i.p.* injected mice (vehicle (normal saline); PAGln (50 mg/kg); PAGly (50 mg/kg)) were anesthetized with ketamine and xylazine and subjected to a common carotid artery injury as previously described (Zhu et al., 2016). Rhodamine 6G (100 μL; 0.5 mg/mL) was injected directly into the right jugular vein to label platelets. The left carotid artery was exposed and injured by placing 1.5 × 1.5 mm^2 Whatman filter paper soaked in 10% $FeCl_3$ solution to the surface of the vessel for 1 min. After removing the paper, the vessel was covered with saline. Thrombus formation was observed in real time using intravital fluorescence microscopy equipped with video recording. Time to cessation of blood flow through clot formation for all studies was determined by visual inspection by two independent investigators.

Dynamic Mass Redistribution (DMR) Studies on MEG01 and HEL Cells

MEG01 and HEL92.1.7 cells were grown in RPMI 1640 media supplemented with fetal bovine serum (FBS; 10%), penicillin (100 U/mL) and streptomycin (100 μg/mL) in a humidified atmosphere at 37°C in 5% CO_2. Prior to a DMR experiment, cells were incubated in a reduced serum media (Opti-MEM) overnight. The following morning, Opti-MEM was removed and cells were washed with 1X HBSS buffer with HEPES (20 mM; pH 7.4), and seeded into a 96-well fibronectin coated epic corning DMR plate (Corning) at a density of 80,000-100,000 cells per well suspended in the same buffer (100 μL). The DMR plate was briefly centrifuged (100 x *g* for 10-15 s at r.t.) to allow the cells to settle at the bottom of the plate and then kept at room temperature for 1 h at room temperature prior to the DMR measurements. In a typical DMR experiment, basal DMR responses were first collected for 15 min to confirm flat baseline DMR responses and this was defined as the zero point. For the DMR dose response experiments, increasing concentrations, as indicated of the compound of interest (25 μL; 5X concentration) (PAGln, Norepi or Phe) or vehicle (25 μL) were added and the DMR signal was read for 60-90 min in a Corning Epic BT system (Corning Epic). DMR studies using G-protein modulators were performed by preincubation the cells with pertussis toxin (PTX; 100 ng/mL) for 30 min, cholera toxin (CTX; 1 μg/mL) for 45 min, YM-254890 (0.5 μM) for 30 min or SCH-202676 (1 μM) for 30 min, as indicated before the addition of the compound of interest (PAGln (100 μM), Norepi (10 μM) or collagen (10 μg/mL)). Loss of function DMR studies with siRNAs on MEG01 cells were carried out by transfecting the cells with the indicated *ADRA2A*, *ADRA2B*, *ADRB2* and negative control scrambled Silencer Select siRNAs (combination of 3 siRNAs for each gene; Silencer select human GPCR siRNA (Thermo Fisher, Ambion)) at a concentration of 1 pmol of each of the three siRNAs per well in 96-well DMR plates using the RNAi transfection protocol suggested by the manufacturer (Silencer Select human GPCR siRNA library V4 protocol 2013 –Ambion- Lipofactamine RNAiMAX-Invitrogen). The siRNA transfected cells were analyzed by DMR 40 h post transfection in the presence of the compound of interest (e.g., PAGln (100 μM), epinephrine (10 μM) or ATP (50 μM)). Pharmacological loss of function studies: DMR studies with adrenergic receptor (ADR) inhibitors on MEG01 cells were performed by treating the cells with either vehicle, ICI118,551 (10 μM), propranolol (10 μM) or RX821002 (10 μM) for 30 min as indicated before addition of the compound of interest (e.g., PAGln (100 μM), ISO (10 μM), B-HT933 (50 μM) or ATP (50 μM)). In all cases, DMR response signals were recorded for 60-90 min post compound of interest addition. The maximum DMR response of a test compound alone (e.g., PAGln, Norepi, Epi, ISO, Collagen or ATP) was normalized to 100% in all the DMR experiments performed on suspension cells.

Cell Plasma Membrane Preparations for Binding Experiments

Membranes were prepared as previously described (Naga Prasad et al., 2001). Cell monolayers of CHO-K1 and HEK293 cells were scraped in osmotic buffer (0.6 mL; 25 mM Tris-HCl; pH 7.5; 5 mM EDTA, 2 μg/mL leupeptin and 2 μg/mL aprotinin) and disrupted further by using a Dounce homogenizer. Intact cells and nuclei were removed by centrifugation at 1,000 × *g* for 5 min at 4°C. The collected supernatant was further subject to a centrifugation at 38,000 × *g* for 25 min at 4°C. The pellet was re-suspended in binding buffer (75 mM Tris-HCl (pH 7.5), 10 mM $MgCl_2$, 5 mM EDTA) and used as the plasma membrane fraction. Isolated washed platelets also underwent similar procedures to obtain plasma membrane fraction.

Determination of β2-ADR Density by [^{125}Iodo]-(-)-Cyanopindolol ([^{125}I]-CYP) Binding

β2-ADR density was determined using membrane fractions of the cells/platelets by radioligand binding as previously described (Naga Prasad et al., 2001). Total binding was determined in the presence of 42.75 fmol of [^{125}I]-CYP alone, and nonspecific binding was determined using 42.75 fmol [^{125}I]-CYP plus 10 μM propranolol. The assay was performed in binding buffer at 37°C for 1 h. The membranes were harvested on glass fiber (Brandel, Gaithersburg MD) using a membrane harvester (Brandel, Gaithersburg, MD). The unbound radioisotopes were removed by washing the filter with wash buffer (10 mM Tris-HCl (pH 7.5), 5 mM EDTA) under vacuum. The glass fiber discs were then dried and the radioactivity was measured using a gamma counter (ICN Biomedicals, Costa Mesa, CA). Receptor density was calculated by subtracting the nonspecific binding of [^{125}I]-CYP in the presence of propranolol from specific receptor binding of [^{125}I]-CYP in the absence of propranolol, taking specific activity of the radioisotope into consideration. The receptor numbers were expressed as fmol of receptor per mg of membrane protein.

Dynamic Mass Redistribution (DMR) Studies on Adherent Cells

DMR experiments in the adherent HEK293 cells were carried out on parental HEK293, α2B-HEK293 (stably transfected) and β2-HEK293 (stably transfected) cells by seeding them into EPIC-Corning fibronectin coated 96-well DMR microplates (Corning) at a density of 50,000 cells per well. Cells were grown in DMEM (100 μL) media supplemented with FBS (10%), penicillin (100 U/mL) and streptomycin (100 μg/mL) in a humidified atmosphere at 37°C in 5% CO_2 for 1 day before proceeding with the DMR experiments. For gain of function studies with the α2A ADR, parental HEK293 cells were transfected with either pcDNA3.1(+)-N-DYK empty vector or with pcDNA3.1(+)-*ADRA2A*-N-DYK clone using Lipofactamine 3000 Transfection kit (Invitrogen). Equivalent transfection efficiency for each well was monitored using a GFP reporter (pmaxGFP, Lonza, CH) and was ~80%. DMR studies were performed on transiently transfected cells 2 days post transfection. Prior to performing the DMR measurements, cells were washed with 1X HBSS buffer with HEPES (20 mM, pH 7.4) and allowed to temperature equilibrate for 1 h at room temperature in the same buffer (100 μL). Basal DMR responses were captured for 15 min to obtain a baseline reading that was defined as zero level, and also ensured signal stability. The DMR signal was monitored after adding the compound of interest (final concentrations, e.g., PAGln (100 μM), ISO (10 μM), B-HT933 (50 μM) or ATP (50 μM) as indicated) for 60-90 min. For inhibitor studies, either ICI118,551 (10 μM), propranolol (10 μM) or RX821002 (10 μM) as indicated, were incubated with cells for 30 min before addition of the compound(s) of interest. In all DMR experiments performed on adherent cells, the DMR response (pm shift) to a test compound alone (e.g., PAGln, ISO or BHT933) or in combination with inhibitor/modulator was normalized to the ATP DMR response (a non-ADR GPCR (i.e., P2Y) agonist that is expressed on nearly all cells).

Real-time (RT) PCR of ADR Gene Expression in MEG01 Cells

Total RNA was isolated from MEG01 cells using a TRIZOL RNA isolation protocol 40 h post siRNA transfection. Reverse Transcription was performed using a High-Capacity RNA to cDNA kit (Applied Biosystem) per the manufacturer's recommended protocol. Real time (RT) PCR was carried out following the TaqMan Gene Expression Assays protocol using RT primers and probes of *ADRA2A* (Hs01099503_s1), *ADRA2B* (Hs00265081_s1) and *ADRB2* (Id Hs00240532_s1) from ThermoFisher Scientific.

cAMP Assay in MEG01, Platelets and HEK293 Cells

Intracellular cAMP levels were measured using CatchPoint Cyclic-AMP Fluorescent Assay Kit (Molecular Devices). Briefly, MEG01 cells were washed with 1X HBSS buffer with HEPES (20 mM; pH 7.4) and re-suspended in stimulation buffer (1X HBSS, HEPES (20 mM); pH 7.4, IBMX (0.5 mM), Rolipram (0.1 mM) and BSA (0.1%)). The cells were further seeded into 96 well cell culture plates at a density of 100,000 cells per well (100 μL). Similarly, washed human platelets were re-suspended gently in stimulation buffer and seeded into a 96-well cell culture plates at 4-6 million platelets per well (100 μL). Both the MEG01 cells and platelets were kept thereafter in a 37°C incubator for 10 min before addition of the inhibitors or test compounds as indicated. Where indicated 10 μL (10X concentration) of modulators/inhibitors (when necessary) were added and kept for 15 min at 37°C. After that, 10 μL (10X concentration) of the test compounds (PAGln (100 μM) or ISO (10 μM)) were added and incubated for different time periods at 37°C. The test compounds and the inhibitors/modulators were made in buffer T (1X HBSS, HEPES (20 mM); pH 7.4, IBMX (0.5 mM) and Rolipram (0.1 mM)). The reaction was stopped by adding 50 μL of lysis buffer (provided in the kit, CatchPoint Cyclic-AMP Fluorescent Assay Kit (Molecular Devices)), supplemented with IBMX (0.5 mM) and Rolipram (0.1 mM)) and agitated for 10 min in a plate shaker to facilitate cell lysis. Lysed cells were immediately assayed for cAMP. For the quantification of cAMP, the lysed sample (40 μL), buffer control and cAMP calibrators were added to the appropriate wells of the provided 96-well clear bottom, black walled cAMP assay plates. Next, reconstituted rabbit anti-cAMP antibody (40 μL) was added to all the wells and mixed for 5 min on a plate shaker to ensure mixing. In the next step, reconstituted HRP-cAMP conjugate (40 μL) was added to every well, mixed properly and kept at room temperature for 2 h. The plate contents were aspirated thereafter and washed with wash buffer (300 μL (provided in the kit)) 4 times. After removal of the 4th wash buffer, spotlight red substrate (provided in the kit) was added to each well. The plate was covered with aluminum foil and left at room temperature for at least 10 min before reading fluorescence intensity in a FlexStation 3 Multi-Mode Microplate Reader (Molecular Devices). For cAMP assay with G-protein modulator, pertussis toxin (PTX; 100 ng/mL) was incubated for 45 min, cholera toxin (CTX; 1 μg/mL) was incubated for 60 min, YM-254890 (0.5 μM) was incubated for 45 min or SCH-202676 (1 μM) was incubated for 45 min by adding 10 μL (10X concentration) of each modulators per well prior to addition of the test compound. Notably, in contrast to the action of PTX, CTX lead to permanent activation of adenylyl cyclase resulting in constitutive cAMP production. Since $G\alpha_s$ protein has no

selective inhibitor known to date, CTX was used for investigating signaling through $G\alpha_s$ pathway. In the context of our current experimental design and analysis, CTX addition results in stimulation of adenylyl cyclase and a sustained increase in cAMP, which was considered as the normalized baseline. Addition of any agonist over this baseline value now does not lead to detectable increase in the $G\alpha_s$ subunit driven cAMP production, thereby resulting in masking of the signaling process. Moreover, CTX incubation was performed for at least 60 min before treating with PAGln. A primary reason for longer CTX exposure is to saturate the response through $G\alpha_s$. The cAMP assay with ADR inhibitors in MEG01 cells was performed by treating the cells with ICI118,551 (10 μM), propranolol (10 μM) and RX821002 (10 μM) by adding 10 μL (10X concentration) of the respective inhibitors per well for 15 min before addition of the compound of interest. For cAMP assay in adherent cells, parental HEK293, and β2-HEK293 (stable) cells were seeded into 96-well cell culture microplates with approximately 50,000 cells per well in DMEM (100 μL) media supplemented with FBS (10%), penicillin (100 U/mL) and streptomycin (100 μg/mL) in a humidified atmosphere at 37°C in 5% CO_2. Cells were grown for 24 h before proceeding with cAMP quantification following the same methodology as described for MEG01 cells. For cAMP assays in CHO-K1 cells, parental, empty vector and *ADRB2* transfected cells were prepared as described above for HEK293 cells. Transfected cells were cultured 48 h post transfection before proceeding with quantification of cAMP for cells treated with the indicated compounds using the same procedure to measure cAMP in CHO-K1 cells as described for MEG01 cells. Equivalent transfection efficiency for each well was monitored using a GFP reporter (pmaxGFP, Lonza, CH) and was ~80%.

Intracellular Ca^{2+} Measurement

Intracellular Ca^{2+} in MEG01, HEL92.1.7, parental HEK293, *ADRB2* stably transfected HEK293 (β2-HEK293) cells, empty vector (EV) transfected HEK293 cells, *ADRA2A* (α2A-HEK293) and in *ADRA2B* stably transfected HEK293 (α2B-HEK293) cells was measured using the FLIPR Calcium 5 Assay Kit- Molecular devices (Cat. R8186). Briefly, 100,000 cells per well for suspension cells or 50,000 cells per well for adherent cells were seeded into 96 well clear bottom, black walled cell culture plates (Falcon) in assay buffer (100 μL; 1X HBSS, 20 mM HEPES, pH 7.4). Adherent cells were grown for 1 day prior to the experiment. Calcium assay reagent component A (provided in the kit) was re-suspended in Component B (10 mL; provided in the kit) and mixed by vortexing for 1 to 2 min to prepare the loading buffer. Probenecid (100 μL of a 250 mM stock) was added in the loading buffer before proceeding with the assay. Loading buffer (100 μL) was added to each well of the 96 well plate. The plates were incubated for 1 h at 37°C and thereafter kept at room temperature until used for the assay. A test compound 96-well microplate was prepared adding 5X concentration of the compound of interest (final concentrations: PAGln (100 μM), ADP (10 μM) or TFLLR-NH_2 (10 μM) in appropriate wells. To start the assay, 50 μL of the 5X test compounds were added to the assay plates in the respective wells in a FlexStation 3 Multi-Mode Microplate Reader (Molecular Devices). The [Ca^{2+}] level was monitored in real time post compound addition as relative fluorescent unit (RFU). The maximum RFU peak minus minimum base line RFU was used as the net measurement of [Ca^{2+}] level.

QUANTIFICATION AND STATISTICAL ANALYSIS

To examine the differences between groups, we used Student's t test (2 tailed) or Wilcoxon's rank-sum test for continuous variables, and $\chi 2$ test for categorical variables. Rank-based nonparametric Kruskal-Wallis test was used for non-normally distributed data. In the box-whisker plot, the upper and lower boundaries of the box represent the 25th and 75th%iles, the median is marked by a horizontal line inside the box, and whiskers represent 10%ile and 90%ile of measured values. Categorical data are presented as n (%). Hazard ratio (HR) for MACE at 3-year follow-up and corresponding 95% confidence intervals (CI) were estimated using both univariable (unadjusted) and multivariable (adjusted) Cox models. Kaplan–Meier analysis with Cox proportional hazards regression was used for time-to-event analysis to determine HR and 95% CI for MACE. Adjustments were made for individual traditional cardiac risk factors including age, sex, HDL, LDL, triglycerides, smoking, diabetes mellitus, systolic blood pressure, and high-sensitivity C-reactive protein level. All data are presented as mean ± SD or SEM, as indicated. Statistical tests used to compare conditions are indicated in figure legends. GraphPad PRISM version 8.0 and R 3.4.2 (Vienna, Austria, 2017) were used for generation of graphs and statistics.

DATA AND CODE AVAILABILITY

There are restrictions to the availability of clinical data generated in this study as we do not have permission in our informed consent from research subjects to share data outside of our institution without their authorizations.

ADDITIONAL RESOURCES

Patient samples and clinical data used for the Discovery Cohort, and the independent Validation Cohort, were obtained from the study entitled GeneBank at the Cleveland Clinic: Molecular Determinants of Coronary Artery Disease (GATC), which was performed under an approved protocol registered under ClinicalTrials.gov Identifier: NCT00590200. Antibiotic suppression of gut microbial metabolite levels in humans were performed under an approved protocol registered under ClinicalTrials.gov Identifier: NCT01731236.

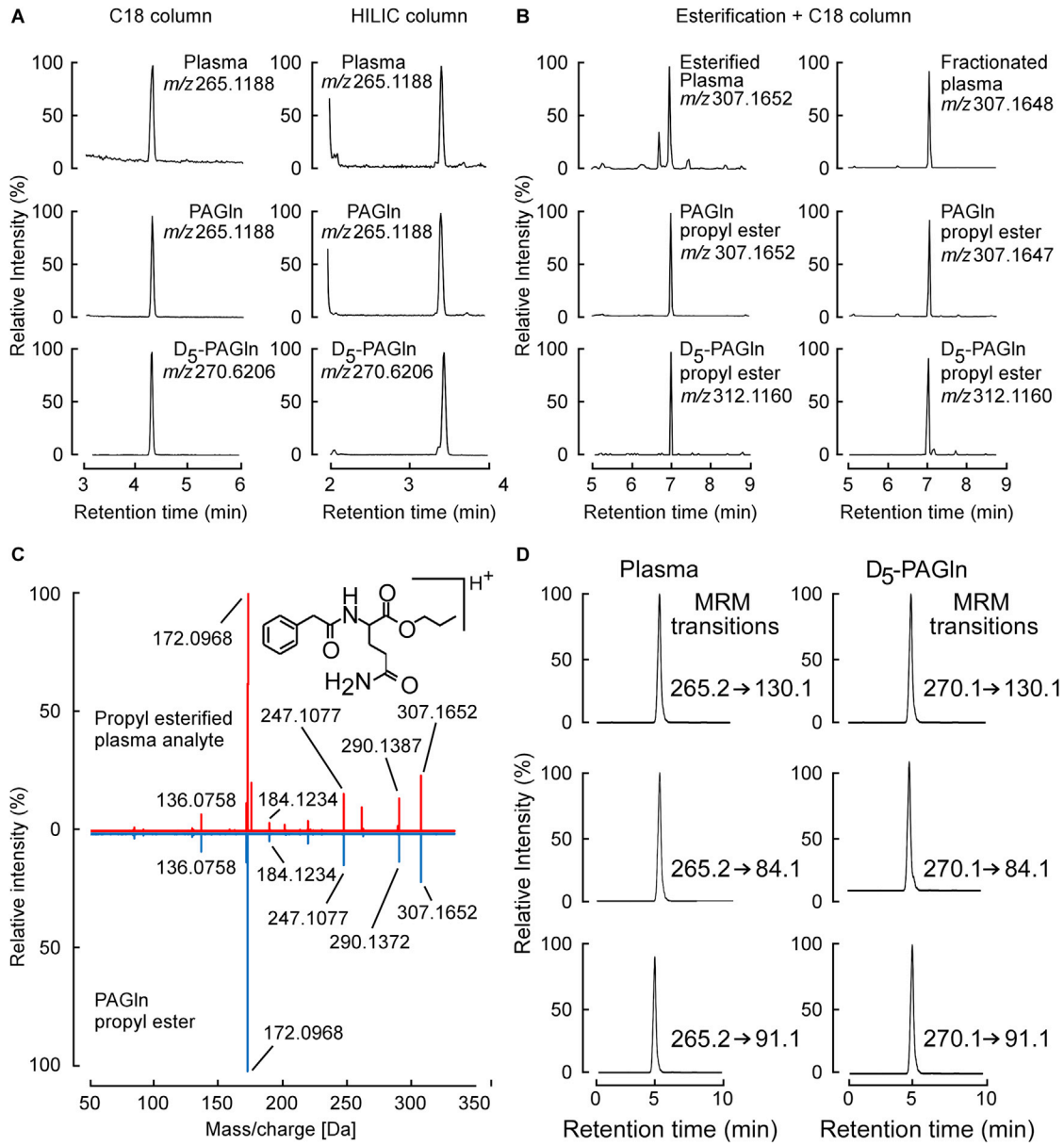

Figure S1. Structural Confirmation of Phenylacetylglutamine, Related to Figure 1

(A) Demonstration of co-chromatography of analyte *m/z* 265.1188 within a plasma sample, and from synthetic PAGln and D_5-PAGln run on UHPLC in tandem with a high-resolution mass spectrometer on two different columns (reverse phase [C18] column [left] and normal phase [HILIC] column [right]).

(B) Demonstration of co-chromatography following derivatization of candidate plasma analyte *m/z* 265.1188, which shifted to *m/z* 307.1652, similar to behavior of authentic synthetic PAGln and the isotopologue D_5-PAGln. The purified analyte in plasma with *m/z* 265.1188 (right) and synthetic PAGln and D_5-PAGln were esterified with propyl chloroformate in propanol.

(C) Comparison of the high-resolution CID mass spectra in positive ion mode of the propyl chloroformate in propanol derivative of the metabolite in plasma (*m/z* 265.1188), which now demonstrates MH^+ = *m/z* 307.1652 (red) and synthetic phenylacetylglutamine propyl ester (PAGln propyl ester, blue).

(D) Chromatograms generated by multiple reaction monitoring (MRM) transitions for the plasma analyte (*m/z* 265.2) and synthetic isotopically labeled PAGln internal standard (D_5-PAGln; *m/z* 270.1). Both compounds were monitored at 3 different characteristic parent to daughter transitions.

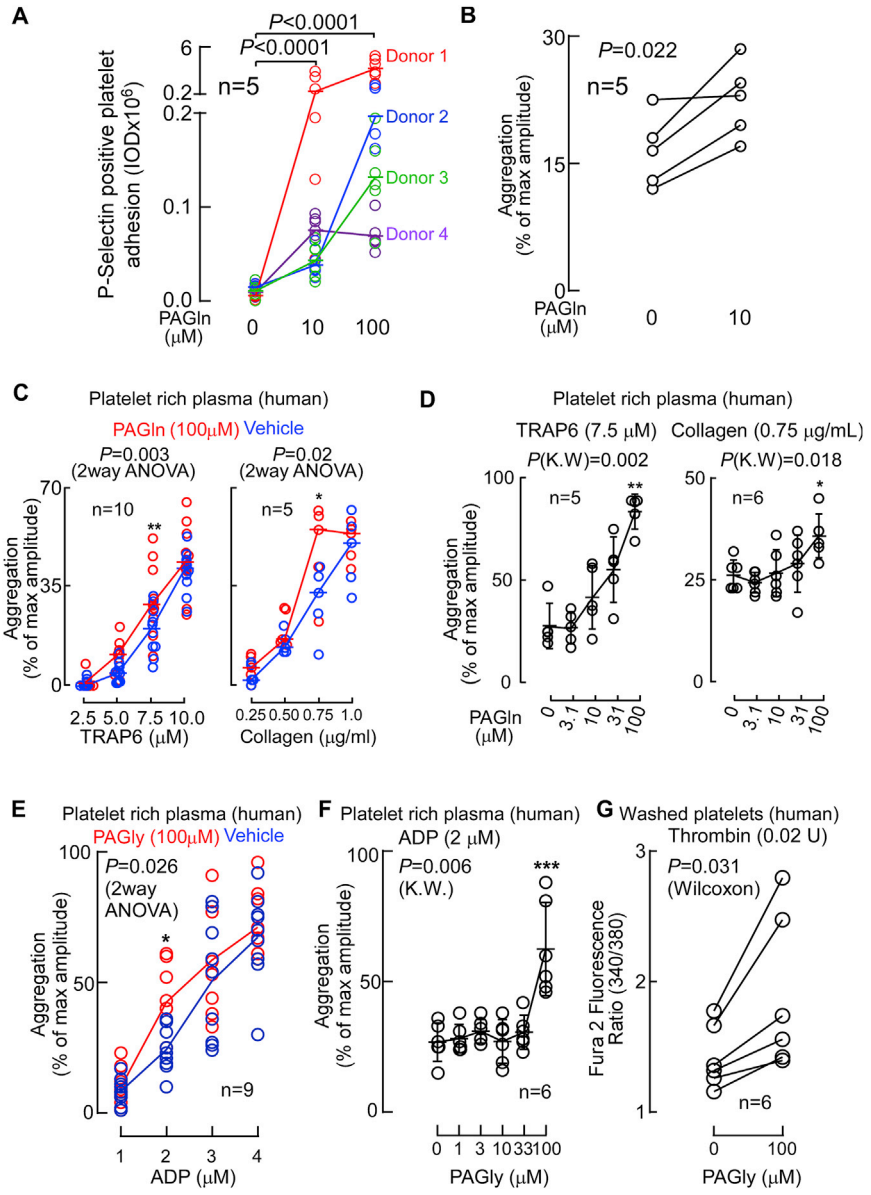

Figure S2. PAGln and Phenylacetylglycine Enhance Platelet Responsiveness, Related to Figure 3

(A) P-Selectin-positive, human platelet (stained with PE-conjugated anti-P-selectin antibody) adhesion in whole blood to a microfluidic chip surface coated with collagen under physiological shear conditions ± the indicated concentrations of added PAGln (n = 5 replicates per donor). Results from (n = 4) donors are shown.

(B) ADP (2 μM)-induced changes in aggregation in PRP pre-incubated with either PAGln 0 μM or PAGln 10 μM at 20°C for 30 min (n = 5 donors).

(C) The impact of PAGln (100 μM) on stimuli-dependent platelet aggregation responses (TRAP6 [n = 10], or collagen [n = 5] at the indicated concentrations).

(D) The impact of increasing concentrations of PAGln on platelet responsiveness (monitored by platelet aggregometry) to submaximal stimulation by TRAP6 (n = 5) or collagen (n = 6) are shown.

(E) PRPs, isolated from healthy volunteers (n = 9), were preincubated with PAGly (100 μM final, red) versus normal saline (vehicle, blue) at 20°C for 30 min, and then platelet aggregometry was used to assess platelet responsiveness to varying dose of ADP for each subject.

(F) At a fixed submaximal level of ADP, the effect of varied levels of PAGly on platelet responsiveness was monitored (n = 6).

(G) Thrombin-induced changes in intracellular calcium concentration [Ca^{2+}] in Fura 2-filled washed human platelets (n = 6) incubated with vehicle or PAGly (100 μM).

Significance was measured with nonparametric one- or two-way ANOVA and Wilcoxon paired test. Data points represent the mean ± SEM (n = biological replicates).

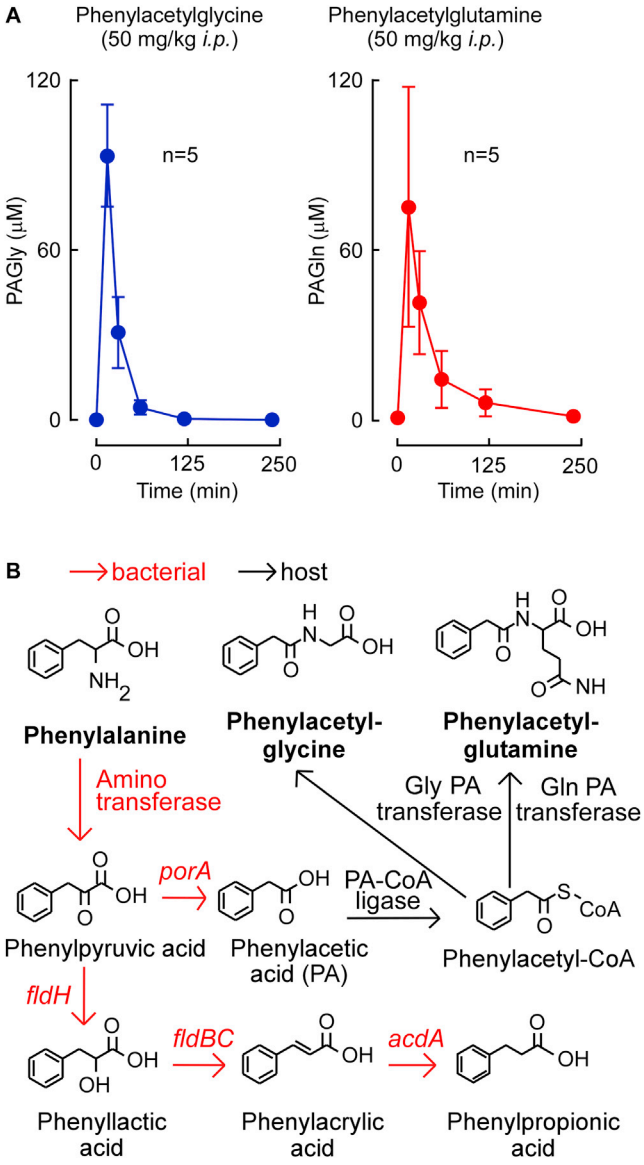

Figure S3. Related to Figure 4

(A) Levels of PAGly (n = 5, left) and PAGln (n = 5, right) in mouse plasma after i.p. injection (50 mg/kg) over time.

(B) Proposed metaorganismal pathway for production of PAGly and PAGln.

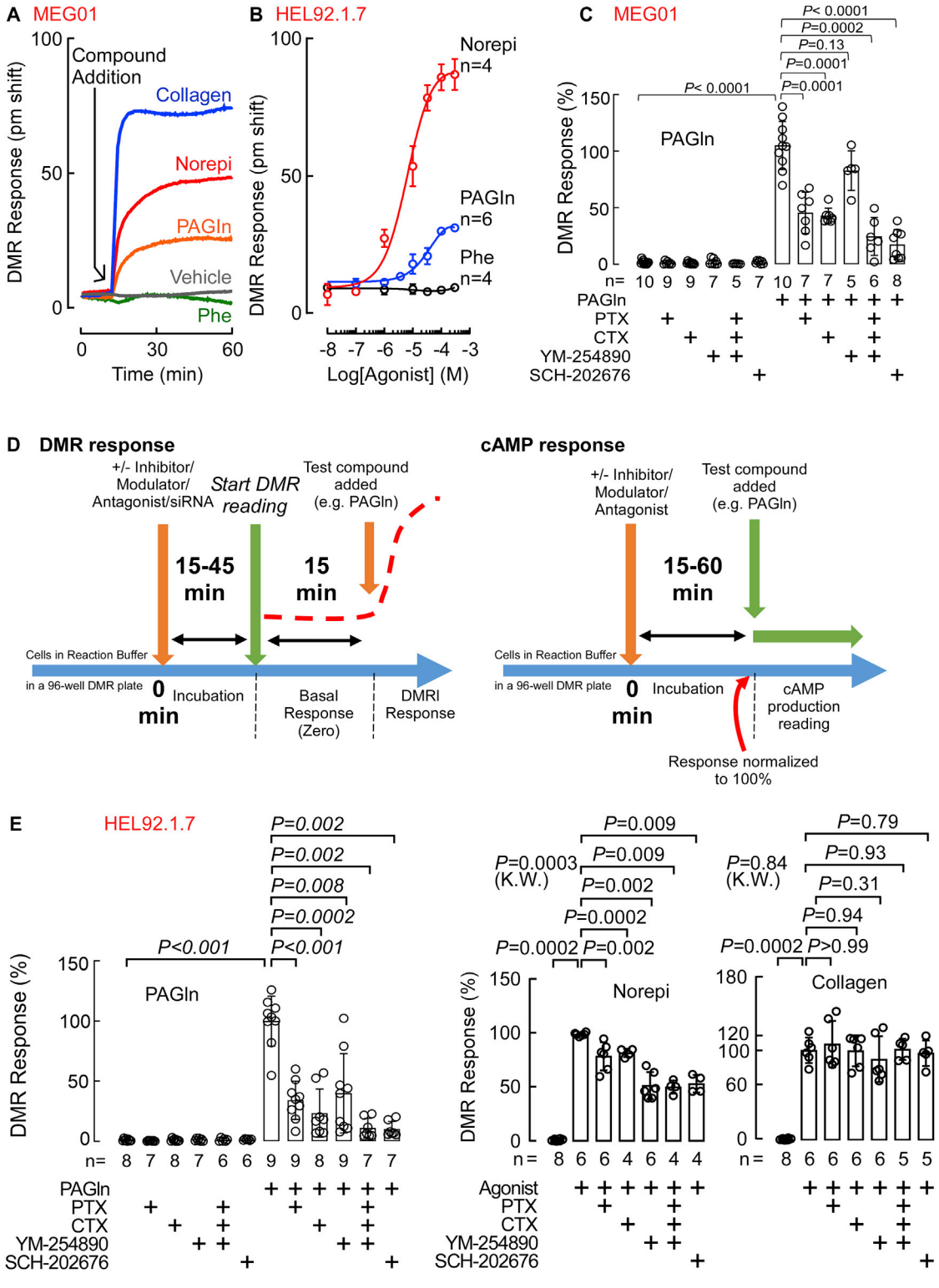

Figure S4. Related to Figure 5

(A) In MEG01 cells, a representative DMR response graph over time with the addition of collagen (10 μg/mL), Norepi (10 μM), PAGln (100 μM), or Phe (100 μM) is shown. The maximum response (in Δpm) to a given treatment is used to quantify the DMR response.

(B) DMR dose response of PAGln (n = 6), Norepi (n = 4), and Phe (n = 4) in HEL 92.1.7 cells. Curves were generated quantifying the maximum DMR response after the indicated ligand addition.

(legend continued on next page)

(C) DMR response to 100 μM PAGln in MEG01 cells before and after the treatment with G-protein modulators, PTX (100 ng/mL), CTX (1 μg/mL), YM-254890 (0.5 μM), or SCH-202676 (1 μM) (n = 5–10 as indicated), which masks signaling through $G\alpha_i$-subunit, $G\alpha_s$-subunit, $G\alpha_q$-subunit, or almost all GPCRs, respectively. Values are normalized to maximum DMR response of PAGln, alone.

(D) Schematic describing the timeline of addition of different compounds and incubation periods in DMR experiments with inhibitors, modulators, and siRNAs (left) and schematic describing the timeline of addition of different compounds and incubation period in cAMP measurement experiments with modulators and antagonists (right). Since different biological samples display variable DMR signal magnitude, the maximum DMR response of a test compound was normalized to 100% in all the subjects. cAMP levels were normalized to 100% in all the inhibitor-treated or untreated samples before addition of PAGln or ISO.

(E) DMR response of PAGln (100 μM, left), Norepi (10 μM, middle), and collagen (10 μg/mL, right) in HEL92.1.7 cells after treatment with G-protein modulators, PTX (100 ng/mL), CTX (1 μg/mL), YM-254890 (1 μM), or SCH-202676 (1 μM) (n = 4–9 as indicated). The maximum DMR response of a test compound (PAGln, Norepi, or collagen) normalized to 100% for each experimental group. Significance was determined by nonparametric Mann-Whitney test for non-pairwise comparison and Kruskal-Wallis test for multiple comparisons. Data points represent the mean ± SEM (n = biological replicates).

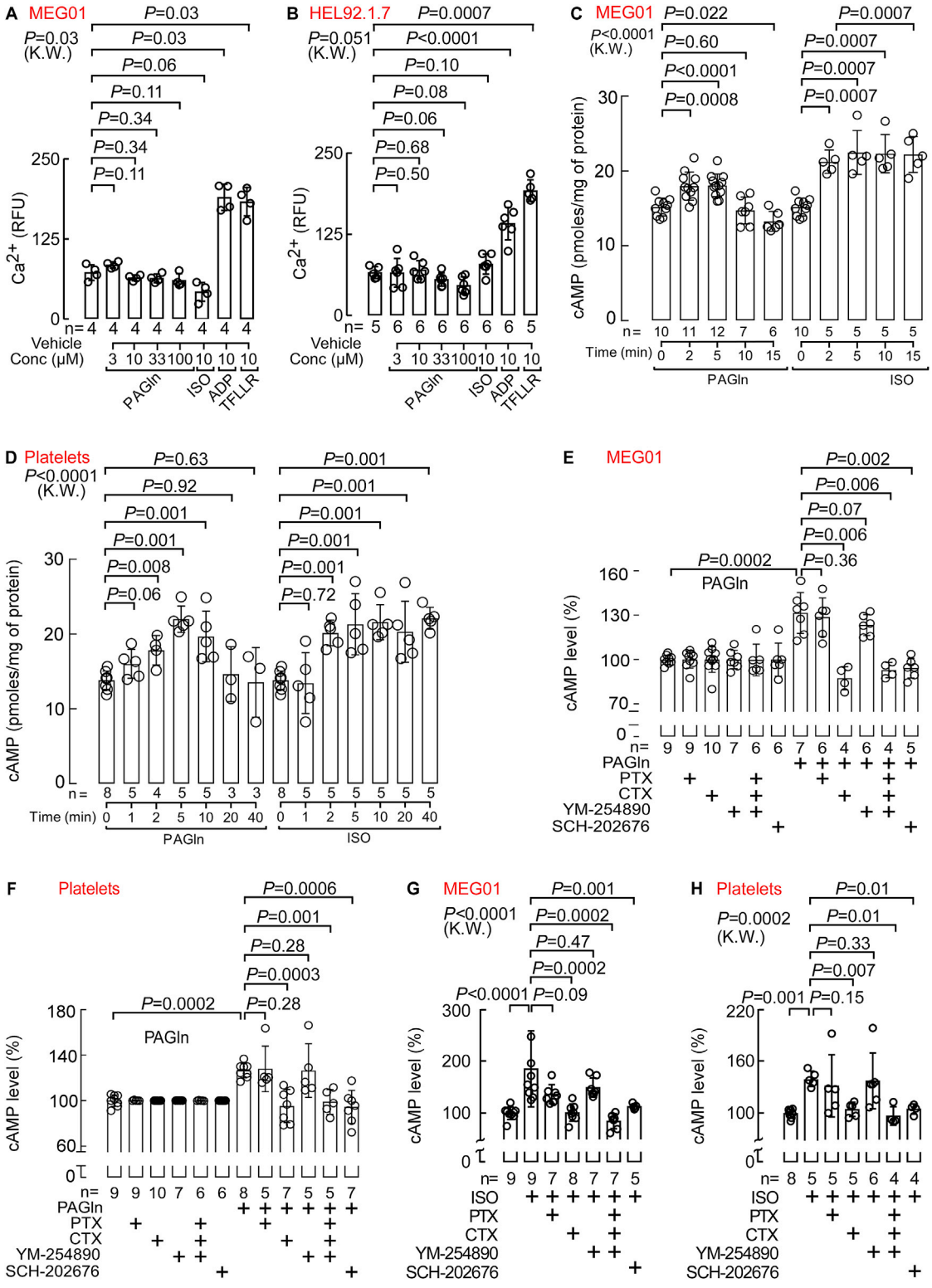

Figure S5. Related to Figure 5

(A and B) Intra cellular Ca^{2+} levels were measured after treating MEG01 cells (n = 4) (A) and HEL92.1.7 cells (n = 5–6 as indicated) (B) with the indicated concentrations of PAGln. ADP (10 μM) and TFLLR-NH_2 (10 μM) were used as positive controls. ISO (10 μM) was used as negative control. Relative fluorescence unit (RFU) was quantified using the maximum peak fluorescence after ligand addition.

(legend continued on next page)

(C and D) cAMP levels in MEG01 cells (n = 5–12 as indicated) (C) and in washed human platelets (n = 3–8 as indicated) (D) were determined at indicated times after treatment with PAGln (100 μM) or with ISO (10 μM) as a positive control. Significance was determined by nonparametric Mann-Whitney test for pairwise comparison and Kruskal-Wallis test for multiple comparisons.

(E and F) cAMP levels in MEG01 cells (n = 4–10 as indicated) (E) and in washed human platelets (n = 5–10 as indicated) (F) after PAGln (100 μM) treatment for 5 min, in the presence of PTX (100 ng/mL), CTX (1 μg/mL), YM-254890 (1 μM), or SCH-202676 (1 μM) as indicated.

(G and H) cAMP levels in MEG01 cells (n = 5–9 as indicated) (G) washed human platelets (n = 4–8 as indicated) (H) after ISO (10 μM for 5 min) treatment in presence of either PTX (100 ng/mL), CTX (1 μg/mL), YM-254890 (1 μM) or SCH-202676 (1 μM) as indicated. Significance was determined by nonparametric Mann-Whitney test for pairwise comparison and Kruskal-Wallis test for multiple comparison. Data points represent the mean ± SEM.

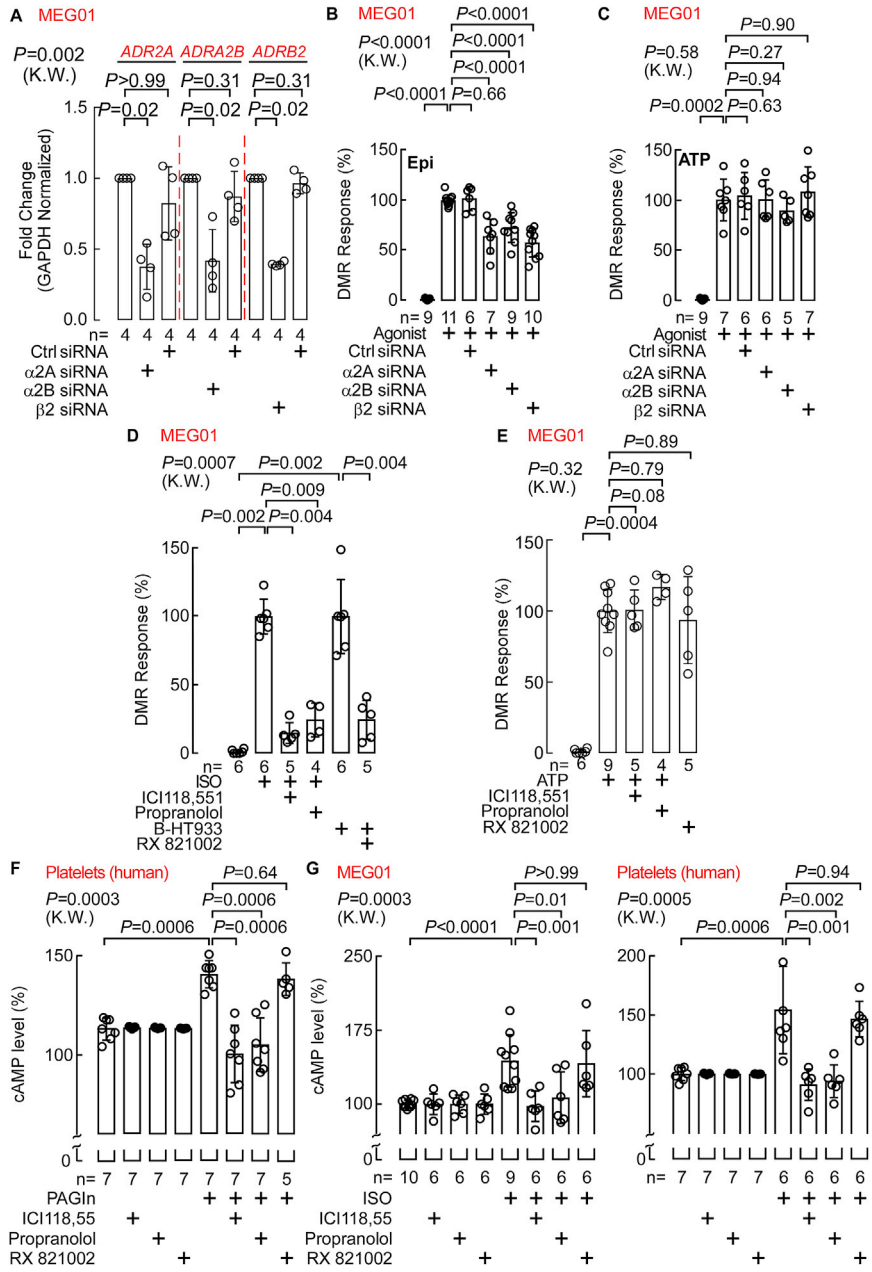

Figure S6. Related to Figure 5

(A) Levels of *ADR2A*, *ADR2B*, and *ADRB2* mRNAs were determined in MEG01 cell lines by quantitative real-time PCR after transfecting the cells with either control scrambled siRNAs or siRNAs against α2A, α2B, and β2 adrenergic receptors as indicated (n = 4).

(B and C) DMR response to Epi (10 μM; n = 6–11 as indicated) (B) and ATP (50 μM; n = 5–9 as indicated) (C) was measured after transfecting the MEG01 cells with control scrambled siRNAs or siRNAs against α2A, α2B, or β2 adrenergic receptors. Maximum response to Epi and ATP were normalized to 100%.

(D) DMR response to ISO (10 μM) (in the presence of selective β2 antagonist ICI118,551 [10 μM] and nonselective beta-blocker propranolol [10 μM]) and B-HT933 (50 μM) (with nonselective α2 antagonist RX821002 [10 μM]) was quantified after treating MEG01 cells with the indicated respective inhibitors for 30 min prior to ISO addition (n = 4–6 as indicated). Maximum response of ISO and B-HT933 were normalized to 100%.

(E) DMR response to ATP (50 μM) in MEG01 cells after 30 min treatment with selective β2 antagonist ICI118,551 (10 μM), nonselective β-blocker propranolol (10 μM), or nonselective α2 antagonist RX821002 (10 μM) (n = 4–9 as indicated).

(F) cAMP levels were measured in washed human platelets (n = 5–7 as indicated) after treating the cells with PAGln (100 μM) for 5 min in the presence of ICI118,551 (10 μM), propranolol (10 μM), or RX821002 (10 μM). cAMP levels were normalized to 100% in all the inhibitor-treated or untreated subjects before addition of PAGln (n = number of biological replicates).

(legend continued on next page)

(G) Measurement of cAMP levels in MEG01 (left; n = 6–10 as indicated) and in washed human platelets isolated from healthy volunteer donors (right; n = 6–7 as indicated) after treating them with ISO (10 μM) for 5 min in the presence of ICI118,551 (10 μM), propranolol (10 μM), or RX821002 (10 μM) as indicated. cAMP levels were normalized to 100% in all the inhibitor-treated or untreated subjects before addition of ISO (n = number of biological replicates). Significance was determined by nonparametric Mann-Whitney test for non-pairwise comparison and Kruskal-Wallis test for multiple comparisons. Data points represent the mean ± SEM.

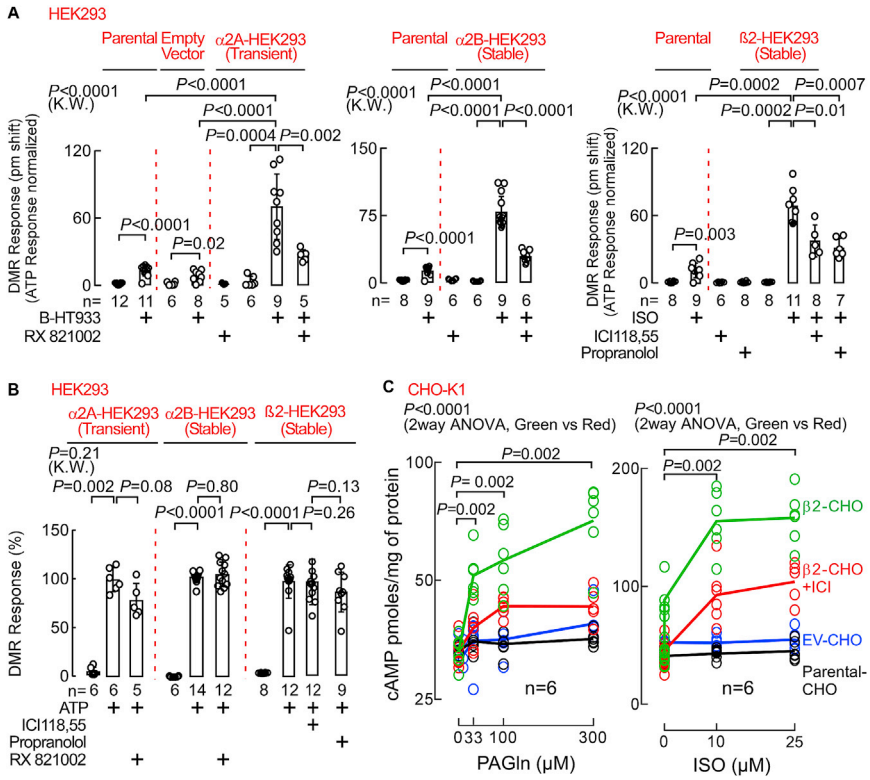

Figure S7. Related to Figure 6

(A) B-HT933 (50 μM; left and middle; n = 5–12 as indicated) and ISO (10 μM; right; n = 6–11 as indicated) DMR response was analyzed in parental HEK293, EV-transfected HEK293, *ADRA2A*-transfected HEK293 (left), α2B-HEK293 stably expressing cells (middle), and in β2-HEK293 stably expressing cells (right) after pretreating the cells with selective β2 antagonist ICI118,551 (10 μM), nonselective beta-blocker propranolol (10 μM), or nonselective α2 antagonist RX821002 (10 μM) for 30 min. (B-HT933 and ISO response was calculated with respect to relative ATP response in all the samples).

(B) ATP (50 μM) DMR response was analyzed as a negative control in *ADRA2A*-transfected HEK293 (left), α2B-HEK293 stably expressing cells (middle), and in β2-HEK293 stable cells (right) after treating the cells with selective β2 antagonist ICI118,551 (10 μM), nonselective β-blocker propranolol (10 μM), or nonselective α2 antagonist RX821002 (10 μM) for 30 min as indicated (n = 5–14 as indicated). (Maximum response to ATP was normalized to 100%).

(C) cAMP level was analyzed in parental CHO-K1 cells (black line), EV-transfected CHO-K1 cells (blue line), *ADRB2*-transfected CHO-K1 cells (green line), and *ADRB2*-transfected CHO-K1 cells along with β2-antagonist ICI118,551 (10 μM; red line), after treating the cells with increasing concentration of either PAGln (left) or ISO (right) for 10 min (n = 6). Significance was determined by nonparametric Mann-Whitney test for non-pairwise comparison and Kruskal-Wallis test for multiple comparisons. Data points represent the mean ± SEM.

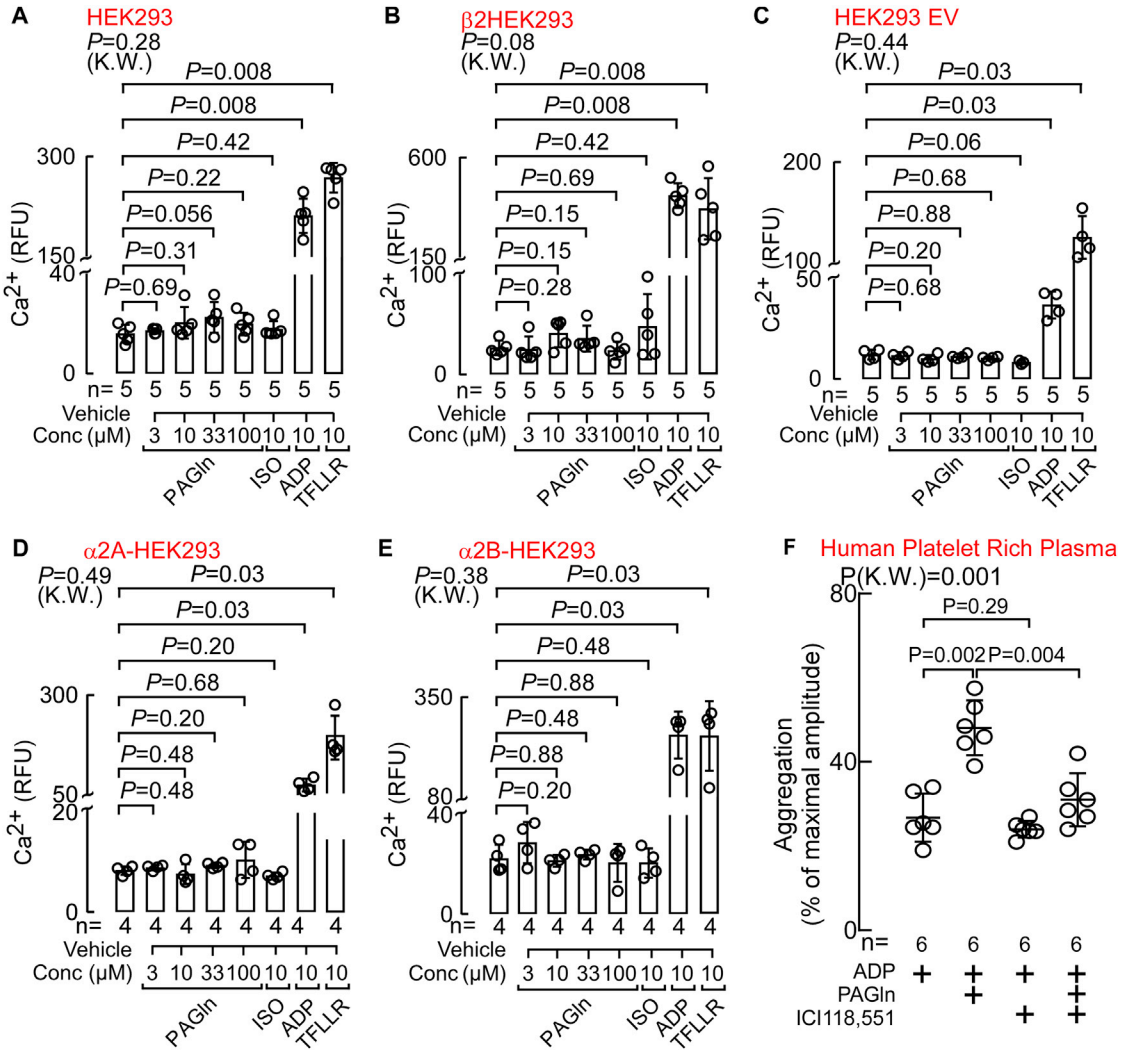

Figure S8. Related to Figure 6

(A–E) Intracellular Ca^{2+} levels were measured in parental HEK293 cells (A; n = 5), β2-HEK293 stably expressing cells (B; n = 5), EV-transfected HEK293 cells (C; n = 5), *ADRA2A*-transfected HEK293 cells (D; n = 4), and α2B-HEK293 stably expressing cells (E; n = 4) treated with the indicated concentrations of PAGln. ADP (10 μM) and TFLLR-NH_2 (10 μM) were used as positive controls for all cells. ISO (10 μM) was used as a negative control. RFUs were quantified using the maximum fluorescence peak after ligand addition.

(F) Platelet aggregation was measured in human PRP (n = 6) preincubated with selective β2-blocker ICI118,551 (10 μM) for 15 min followed by PAGln (100 μM) for 30 min before stimulation with a submaximal concentration of ADP (2μM). Data points represent aggregation as the percentage of maximum amplitude in PRP recovered from each human subject. Significance was determined by nonparametric Mann-Whitney test for non-pairwise comparison and Kruskal-Wallis test for multiple comparisons. Data points represent the mean ± SEM (n = number of biological replicates).